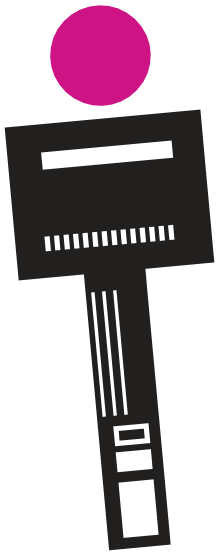

RAM ROBOTICS AND MECHATRONICS

DEVELOPMENT OF A BLADDER PHANTOM TO USE WITH OCT AND MINIATURE CAMERA EXPERIMENTS PERFORMED BY THE ROBOT-CONTROLLED CATHETER OF THE NEXT-GEN IN-VIVO PROJECT

A.C. (Alies) ter Lingen

BSc assignment

Committee:
dr. F.J. Siepel
dr. V. Groenhuis
dr. M. Dantuma

August, 2022

027RaM2022
Robotics and Mechatronics
EEMCS
University of Twente
P.O. Box 217
7500 AE Enschede
The Netherlands

UNIVERSITY OF TWENTE. | TECHMED CENTRE

UNIVERSITY OF TWENTE. | DIGITAL SOCIETY INSTITUTE

Abstract

The global bladder cancer mortality rate of 212.536 (2020) can be reduced when diagnostic techniques are improved [1]. For the Next-Gen In-Vivo project a robot-controlled catheter is developed that uses Optical Coherence Tomography (OCT) and a miniature camera to make a 3D reconstruction of a bladder to easily localize and categorize a bladder tumour. To test this new diagnostic technique a phantom that represents the characteristics of a human bladder is necessary. In this report the development of such a bladder phantom is described. The inclusion of the different bladder layers, urothelium, lamina propria and muscularis propria, and different bladder tumour types is investigated. Each bladder layer and tumour type has its own optical properties. These optical properties were achieved by mixing different concentrations of scattering agents into a base material for each layer and tumour. Three different base materials, namely Dragon Skin, Ecoflex and plastisol, and two different scattering agents, namely titanium dioxide and silica, were used. Different combinations of these base materials and scattering agents were tested for the creation of a bladder phantom. A new fabrication process has been developed by combining existing methods for the creation of (bladder) phantoms and including new techniques. In short, the sandwich moulding technique is used whereby different numbers of aluminium foil layers are wrapped around the inner part of the mould to fabricate a textured semi-spherical wall phantom, consisting of layers that have thicknesses that are normally too small to be achieved by the sandwich moulding technique. In separate test pieces the different bladder tumour types were included. The phantoms and tumour test pieces were imaged by OCT, ultrasound and a miniature camera. The OCT images did not show a three-layered structure, but many of the ultrasound images did. Therefore, the intensities and thicknesses of the layers could be evaluated for the different phantoms and the tumour characteristics for the different test pieces by using the ultrasound scans. Moreover, the texture of the inner surfaces of the phantoms was visualised by the miniature camera and compared to the lining of a human bladder. Some further improvements have to be made to make the phantoms even more realistic, but a proper new prototype of a phantom to use for tests with the robot-controlled catheter has been made.

Nederlandse samenvatting

De wereldwijde sterfte veroorzaakt door blaaskanker van 212.536 (2020) kan verminderd worden door verbetering van de diagnostische technieken [1]. Bij het Next-Gen In-Vivo project wordt een katheter ontworpen die door een robot aangestuurd wordt en gebruik maakt van de beeldvormende techniek Optical Coherence Tomography (OCT) en een miniatuur camera om een 3D reconstructie van een blaas te maken om hiermee een blaastumor makkelijk te kunnen lokaliseren en categoriseren. Om deze nieuwe diagnostische techniek te testen is een fantoom nodig dat de eigenschappen van een menselijke blaas nabootst. In dit verslag wordt de ontwikkeling van zo een blaasfantoom beschreven. Er is onderzocht hoe de verschillende lagen van de menselijke blaas, urothelium, lamina propria en muscularis propria, en verschillende typen blaaskanker tumoren in het fantoom verwerkt kunnen worden. Elke laag van de blaas en elk tumor type bevat specifieke optische eigenschappen. Het nabootsen van deze optische eigenschappen is gebeurd door voor elke laag en tumor verschillende concentraties van verstrooiing inducerende deeltjes te mengen in een basis materiaal. Er zijn drie verschillende basis materialen, namelijk Dragon Skin, Ecoflex en plastisol, en twee verschillende verstrooiing inducerende deeltjes, namelijk titanium dioxide en silica, gebruikt. Verschillende combinaties van basis materialen en verstrooiing inducerende deeltjes zijn onderzocht met betrekking tot het maken van een blaasfantoom. Een nieuw fabricage proces is ontwikkeld door bestaande

methoden voor het maken van een (blaas)fantoom te combineren en vernieuwende technieken toe te voegen. Kort gezegd wordt de sandwich techniek gebruikt waarbij een verschillend aantal lagen aluminium folie om het binnenste deel van de mal gewikkeld wordt om een half-bolvormige wand die textuur bevat te fabriceren dat geldt als fantoom en bestaat uit lagen die een dikte hebben die normaal te klein is om te maken met de sandwich techniek. In losse proefstukjes zijn de verschillende blaastumoren toegevoegd. De fantomen en tumor proefstukjes zijn gescand door OCT, ultrasound en een miniatuur camera. De OCT afbeeldingen lieten geen structuur van drie lagen zien, maar veel van de ultrasound afbeeldingen wel. Daarmee kunnen de intensiteiten en diktes van de lagen bepaald worden voor de verschillende fantomen en de eigenschappen van de tumoren kunnen bepaald worden voor de verschillende tumor proefstukjes aan de hand van de ultrasound scan. Bovendien is de textuur van de binnenkant van de fantomen in beeld gebracht met de miniatuur camera en vergeleken met het binnenste oppervlak van een menselijke blaas. Er zullen nog enkele verbeteringen moeten worden toegepast om het blaasfantoom nog realistischer te maken, maar er is zeker een nieuw, goed prototype fantoom ontwikkeld dat gebruikt kan worden voor experimenten met de robot aangestuurde katheter.

Contents

1. Introduction

In 2020 the bladder cancer incidence worldwide was 573.278 [1]. This results in bladder cancer being the 10th most common cancer globally. Unfortunately, not everyone who is diagnosed with bladder cancer can receive sufficient treatment. The total global bladder cancer mortality rate in 2020 was 212.536 [1]. The stage of the bladder cancer when a patient is diagnosed significantly influences the survival rate [2]. Therefore, it is important to develop a technique that can improve the diagnosis process of bladder cancer.

1.1. Problem description

At the Robotics and Mechatronics group of the University of Twente the Next-Gen In-Vivo project focusses on an image-guided diagnostic technique for bladder cancer [3]. It is important to establish the type of bladder cancer before a suitable treatment plan can be determined. To achieve this, Optical Coherence Tomography (OCT) is used in vivo by bringing an OCT-catheter into the bladder. This minimally invasive surgery provides information to be able to localize and categorize the tumour in patients diagnosed with bladder cancer.

To create physician-independent results and reproducible localisation of the tumour the OCT-catheter should be robot-controlled [3]. Currently, in the Next-Gen In-Vivo project a robot is being developed that is able to make a 3D reconstruction of bladder phantoms through images made by a miniature camera and OCT. However, the phantom that is being used now is very simplistic and made out of cardboard. It would be useful to investigate whether or not the robot-controlled catheter is capable of making a proper 3D reconstructions to localize and categorize a bladder tumour. This can be tested by doing experiments with the robot involving a phantom that better represents the human bladder. This phantom is not available yet. Therefore, the goal is to create a more realistic bladder phantom that can be used in the Next-Gen In-Vivo project. In this report the development and evaluation of such a phantom that includes certain aspects of a human bladder is described.

1.2. Outline report

The report consists of eight chapters. The first chapter is the introduction. Chapters 2 to 4 describe background information obtained by a literature study. This information is needed to be able to make decisions about the materials and methods and thereby the phantom design. Chapter 2 focusses on the anatomy, physiology and pathology, in particular bladder cancer, of the human bladder. In chapter 3 the theory and properties of the three imaging techniques used for the evaluation are addressed. The state of the art regarding (bladder) phantoms is described in chapter 4 as well as the requirements for the developed bladder phantom. The requirements are established by combining the information of the state of the art and the other parts of the literature study. In the last section of chapter 4 the decision process of the phantom design is described, taking the requirements into account. The whole fabrication process is described in chapter 5: Materials and Methods. In this chapter everything that has been done to create the phantoms and test pieces is included. This is needed for the repeatability of the research. The results of the OCT and ultrasound scans and the recordings of the miniature camera are included in chapter 6: Results. Depending on the sample, the intensity, thickness or tumour characteristics were evaluated and noted in chapter 6. The 7th chapter includes the discussion of the results and in chapter 8 conclusions are drawn from the results.

2. Human bladder

For developing a bladder phantom that can be used for testing diagnostic techniques, it is important to first look into the relevant characteristics of a healthy human bladder and bladder cancer.

2.1. Anatomy and physiology

The bladder is a sac that is located in the extraperitoneal space of the pelvis, posterior to the pubic bone [4, 5]. The function of the bladder is to store urine. Urine enters the bladder from the kidneys via the two ureters on the lateral sides of the bladder. The lining of an empty bladder is not smooth, but consists of small folds called rugae. When the bladder is filled with urine it stretches and the rugae diminish. To achieve this elasticity the bladder has a Young's modulus of around 284 kPa. By the time the bladder has reached its maximum capacity of 400 to 600 mL signals are produced to stimulate emptying the bladder. To empty the bladder the muscles in the bladder wall contract, the sphincters (valves) open and the urine flows into the urethra outwards the body.

As depicted in figure 1 the bladder wall consists of three main layers, namely the urothelium, lamina propria and the muscularis propria [4]. The urothelium is the most inner layer and around 50 µm thick. It consists of stratified epithelial cells that can reorganize so the number of cell layers decreases when the bladder stretches. In the middle layer, lamina propria, a lot of different cells and components are present, like capillaries, nerve endings, fibroblasts and elastic fibers. The lamina propria is around 250 µm thick. The most outer and thickest layer, around 1.6 mm thick, of the bladder wall is the muscularis propria, also called the detrusor muscle. This muscle is controlled by the autonomic nervous system so it relaxes when the bladder fills up and contracts when the urine needs to be released. Apart from these three layers of the bladder wall the bladder is covered in connective tissue called serosa or adventitia and in perivesical fat [4].

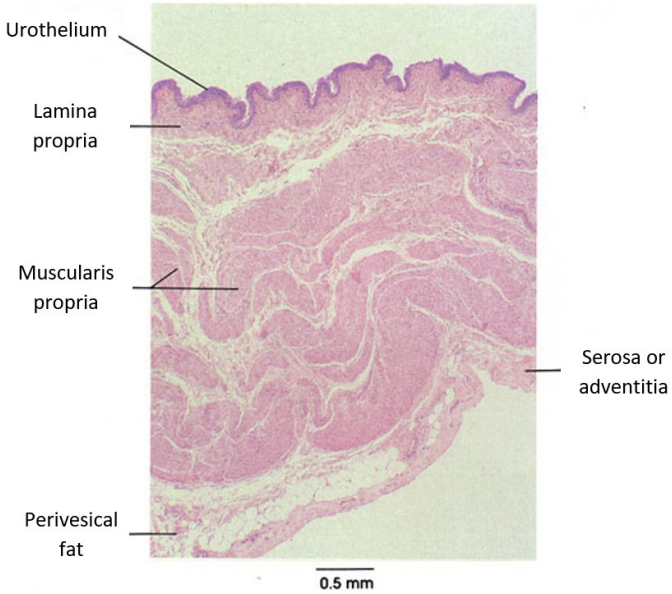

Figure (1) *The bladder wall consists of three layers, namely from inside to outside the urothelium, lamina propria and muscularis propria. The folds in the urothelium and lamina propria are called rugae. Connective tissue, serosa or adventitia, and perivesical fat cover the outside of the bladder [6].*

2.2. Bladder cancer

The treatment of a patient diagnosed with bladder cancer depends on the type of bladder cancer [7]. Therefore, it is necessary that diagnostic techniques are able to distinguish between these types. This can be tested if different bladder tumour types are implemented in a phantom. However, to be able to do this first the different types of bladder cancer that are distinguishable by OCT need to be described.

The TNM system provides a way to describe the stage of a tumour in the bladder [7]. A letter (T, N or M) is used followed by a number or several other letters to classify the tumours in a structured manner. For example, Tis describes the stage of a carcinoma in situ (CIS) [7–9]. This tumour is only infiltrated in the two inner layers of the bladder, the urothelium and the lamina propria. This means that CIS is non-muscle-invasive bladder cancer and therefore treated differently than when the tumour has reached into the muscle layer of the bladder wall. T1 describes a stage where the tumour has spread further into the bladder wall so it also fades the normally clear transition of the urothelium and lamina propria to the muscularis propria [7–9]. The stage of T2 describes a situation of tumour infiltration into the whole bladder wall so the different layers of the bladder wall cannot be distinguished anymore [7–9]. This is a muscle-invasive type of bladder cancer and a different treatment plan needs to be set in motion.

Another type is not described with the TNM system, but called urothelial dysplasia [10]. This is actually not a type of bladder cancer, since it is premalignant. However, dysplasia can be observed through OCT, as will be further discussed in section 3.1. This diagnosis could initiate treatment to prevent the benign tumour becoming malignant. Thus, it is important that diagnostic techniques are able to detect dysplasia so early diagnosis can take place before the possible cancer can grow and spread. Dysplasia is recognized by the thickening of the urothelium in the bladder wall.

3. Bladder imaging techniques

The diagnostic techniques for the detection of bladder cancer that are worked on at the Next-Gen In-Vivo project are based on OCT and recordings of a miniature camera. However, for the more extensive evaluation of the developed bladder phantom described in this report also ultrasound imaging is used. Relevant aspects of these different imaging techniques are discussed for background information and to be able to interpret the results of the evaluations of the bladder phantom.

3.1. Optical Coherence Tomography

For cross-sectional imaging OCT can be used [11, 12]. One of the advantages of using OCT in diagnostics is that there is no need to remove tissue to examine the tissues structure below the surface. Moreover, OCT provides two-dimensional images with resolutions of 1 to 15 µm which is relatively high with respect to for example ultrasound. These images can be made in situ and in real time so fast diagnosis is possible. However, because of optical attenuation in the tissues imaged by OCT, penetration depth is limited to 2 to 3 mm. Luckily this is deep enough to properly diagnose different types of bladder cancer, since the total bladder wall thickness is less than this penetration depth. Besides, for the OCT technique compact fiber optic components can be used which can be integrated in a catheter and thereby brought into the bladder.

OCT uses continuous-wave short coherence length light with wavelengths in the near-infrared [11, 12]. This light is directed onto tissue after which reflection and scattering of the light takes place. Light is back reflected or scattered in structures with different optical properties, for example on boundaries between different types of tissues [13]. The echo time delay and intensity of the back reflected or scattered light are measured [11, 12]. These measurements can be used to determine the axial (longitudinal) distance from where the back reflection or scattering happened and the type of components in the tissue since this depends on optical properties. This information provides the input for the OCT image in which the microstructure of the tissue is visualised. Hereby, parts of the tissue with a low scattering coefficient (μ_s) are displayed with a low intensity in the OCT image and high intensity regions in the OCT image represent parts of the tissue with higher scattering coefficient [11–13].

The different layers in the human bladder wall can be visualised by OCT [8, 9, 14–17]. In figure 2 OCT images of a human bladder wall are shown [8]. In figure 2A the OCT image of a healthy human bladder wall is depicted. In figures 2B, C, D and E the OCT images are shown of a human bladder wall where different bladder tumours invade the wall. Each bladder tumour type as described in section 2.2 is imaged by OCT in these figures. In section 2.1 the three layers of the bladder wall are addressed, namely the urothelium, lamina propria and muscularis propria from the inside to the outside of the bladder respectively [4]. In figure 2 the difference in thickness and intensity of the layers can be noted in the OCT scans. Hereby the urothelium is the thinnest layer with the lowest intensity, the lamina propria is the slightly thicker layer with high intensity and the muscularis propria is the significant thickest layer with low intensity [8, 9, 14–17].

3.2. Ultrasound

Ultrasound is comparable to OCT, except that sound is used for ultrasound imaging instead of light [11, 18]. Sound waves are sent into the tissue where back reflection or scattering takes place due to different acoustic properties of the structures in the tissue. The echo time delay and intensity

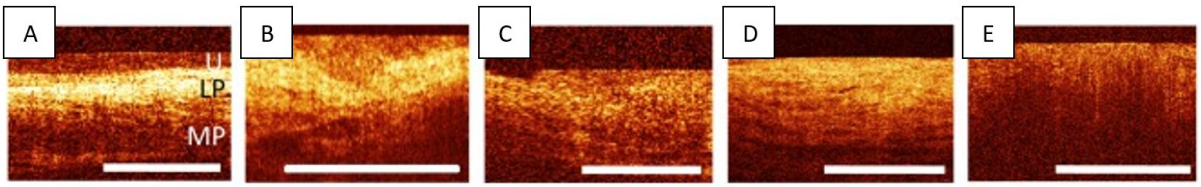

Figure (2) *OCT images of the healthy human bladder wall and of different types of bladder cancer that invade the bladder wall. The different layers in the wall can be distinguished where the upper layer with low intensity represents the urothelium, the middle layer with high intensity the lamina propria and the bottom layer with low intensity the muscularis propria. U: urothelium. LP: lamina propria. MP: muscularis propria. A) Healthy, clearly demarcated layers. B) Urothelial dysplasia, thickened U. C) Carcinoma in situ (CIS), fused U and LP with a clear demarcation with MP. D) T1, fused U and LP without a clear demarcation with MP. E) T2, no clear demarcation between layers [8].*

of the back reflected or scattered sound waves are measured and this information will be converted into the ultrasound image. These cross-sectional images can be made in situ and in real time, just as with OCT. Structures of the tissue that highly scatter the sound waves appear as bright spots on the image while less scattering results in darker parts of the ultrasound image. Ultrasound is a technique that is easier accessible than OCT and therefore also used to evaluate the phantom developed in this report in between opportunities to perform OCT scans.

The image spatial resolution of an ultrasound image and the penetration depth depend on the frequency of the sound wave, higher frequencies achieve higher resolutions but reduce the penetration depth [11, 18]. Low frequency sound waves (10 MHz) limit the image resolution to 150 µm, but can achieve penetration depths up to several tens of centimetres. Therefore, ultrasound can be used to evaluate phantoms with a larger thickness than the penetration depth of OCT. Sound waves of high frequencies (100 MHz) can obtain images with a spatial resolution of 15 to 20 µm, but only visualise structures up to a few millimetres deep within the tissue. Moreover, an ultrasound scan takes longer and transverse resolution of ultrasound are lower than that of OCT. This is because sound waves have a lower velocity and are harder to focus compared to light, respectively. Lastly, the ultrasonic probe transducer needs to be in direct contact with the tissue or transducing medium while OCT can be performed directly through air.

Transabdominal ultrasound can be used to visualise the bladder [19–22]. Such an image is shown in figure 3 [20]. In contrast to imaging the bladder by OCT, ultrasound is performed from the outside of the body. Therefore the distance to the bladder wall is a lot larger and the layers in the bladder wall are not as easily visible with ultrasound as with OCT. Moreover, the lumen of the bladder has a similar intensity on an ultrasound scan as the urothelium which results in the invisibility of the urothelium. As can be seen in figure 3B two layers with high intensity (indicated by the red arrows) and a layer of low intensity in between are visible on an ultrasound scan. The bottom high intensity layer represents the lamina propria and the upper high intensity layer the serosa or adventitia. The low intensity layer in between represents the muscularis propria. This structure of layers complies with the anatomy of the bladder wall described in section 2.1 [4].

No ultrasound images were found in literature where the different types of bladder cancer as described in section 2.2 were shown. However, it can be assumed that the depiction of the different bladder tumour types on ultrasound is comparable to that on OCT, since the visualisation of the healthy bladder wall on ultrasound images is similar to that on OCT images. Only urothelial dysplasia would be harder to visualise, because the urothelium is not easily visible on ultrasound and urothelial dysplasia is characterized by the thickening of the urothelium [10].

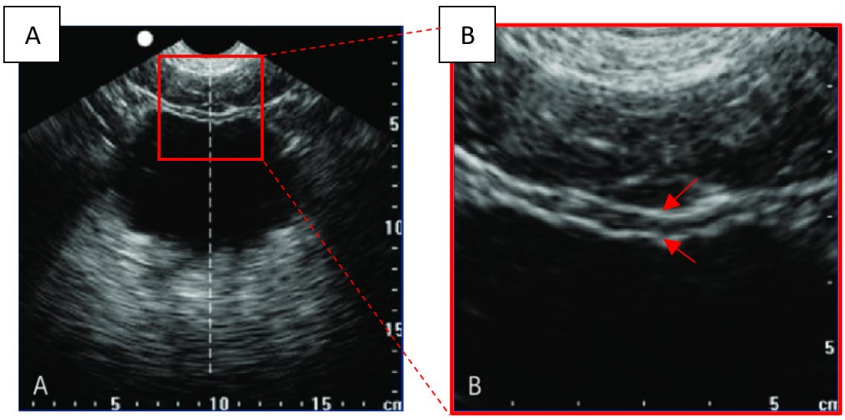

Figure (3) *Ultrasound images of a healthy human bladder. A) Transabdominal ultrasound shows a transverse section of the bladder (dark section). The top part of the image depicts the anterior and the bottom part the posterior side. The red square frames the region of figure B. B) Figure A zoomed-in on the anterior bladder wall. The urothelium is not visible since it its intensity matches the intensity of the bladder lumen. The two layers with the high intensities indicated by the red arrows are the serosa or adventitia (top red arrow) and the lamina propria (bottom red arrow). The layer with the low intensity in between is the muscularis propria [20].*

3.3. Miniature camera

An easy way to look from the end-effectors perspective of the robot-controlled OCT-catheter developed at the Next-Gen In-Vivo project is to attach a miniature camera at the end of the catheter. This camera can be used to investigate if for example the end-effector of the catheter is able to visualise every part of the bladder (phantom) and smooth movements are made. This is more difficult to conclude when OCT is used. Moreover, to this day physicians use White Light Cystoscopy (WLC) as one of the diagnostic techniques to detect bladder cancer [23]. Capturing images with the miniature camera in a room with the lights on can be seen as a form of WLC outside the body.

In figure 4 images of the human bladder created by WLC are shown [24–26]. WLC can be used to visualise the vascularisation and texture of the bladder wall as well as non-muscle invasive bladder cancer [8, 17, 24–26]. Tumours are indicated by red arrows in figure 4. It can be seen that tumours appear as thickened, red spots on the surface of the bladder wall. It is not possible to distinguish the different layers of the bladder wall by WLC, since this technique does not image in depth.

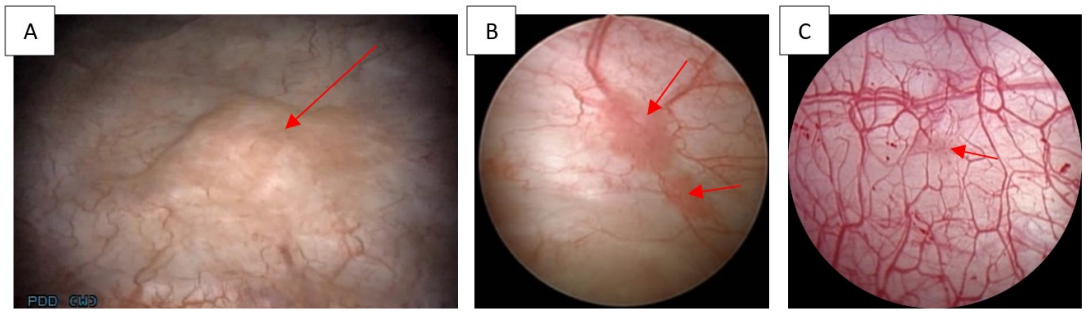

Figure (4) *WLC images of tumorous human bladders. A) Thickening of the bladder wall indicated by the red arrow represents a tumour [24]. B,C) Red spots on the bladder wall indicated by red arrows represent tumours [25, 26].*

4. Bladder phantom

It is useful to determine what has already been researched regarding bladder phantoms and phantoms in general by means of a literature study before the bladder phantom for the Next-Gen In-Vivo project is designed. Subsequently, the state of the art is described. Another important aspect of developing the phantom is to establish the requirements. Finally, decisions about the design of the phantom can be made taking the findings of the literature study, requirements and wishes into consideration.

4.1. State of the art

A literature study has been carried out to determine the state of the art regarding (bladder) phantoms. For the purpose of this report the literature study included previous research concerning bladder phantoms and optically tuned phantoms in general. The findings of the studies have been categorized by base materials, scattering agents and fabrication process and design to describe the possibilities for the creation of (bladder) phantoms that have already been researched.

4.1.1. Base materials

For the development of the phantom it is important that the phantom represents (some of) the optical properties of a human bladder. To achieve this the base material of the phantom should be optically tuneable. Furthermore, it should be possible to deform the base material to create the desired shape for the phantom. In literature multiple materials are described that comply with these requirements. All these materials are optically tuneable by adding scattering agents, described in section 4.1.2, and shaped before the fluid materials cure. Poly(dimethylsiloxane) (PDMS) is an optically clear silicon-based organic polymer used for the creation of phantoms [8, 9, 17]. It cures in 30 minutes at 60 to 90 °C and has a relative high Young's modulus of 800 kPa – 1.72 MPa [8]. Dragon Skin is a material that can be used with a lower Young's modulus, namely 150 kPa – 593 kPa [8]. It cures at room temperature with a curing time varying from 30 minutes to 16 hours depending on the type of Dragon Skin [8]. Another material of the same manufacturer of Dragon Skin is Ecoflex. Ecoflex is less elastic than Dragon Skin. The range of curing times at room temperature depending on the type of Ecoflex is 5 minutes to 4 hours [27]. Multiple articles describe gelatine as a base material for the creation of optically tuned phantoms [28–30]. The optical properties of these phantoms comply with that of a human bladder wall, however the phantoms do not comply with any other characteristics of a human bladder. Sylgard 184 Silicone Elastomer is another material that has been perfectly optically tuned, but not used for the creation of a proper (bladder) phantom yet [31]. The same applies for PVC Plastisol, hereafter called plastisol [32].

4.1.2. Scattering agents

To optically tune the base materials described in section 4.1.1 scattering agents are used. Scattering agents are substances that cause scattering of light. Therefore, when scattering agents are mixed into a material the optical properties of this material changes. The higher the concentration of a scattering agent in a material the higher the scattering coefficient of that material becomes. The scattering agents described in literature used to optically tune the material for the creation of a (bladder) phantom are titanium dioxide, silica particles, polymeric microspheres and Intralipid [8, 9, 17, 28–32]. Most of the base materials include titanium dioxide to create the phantoms, so more is known about the required concentration of titanium dioxide to comply with the scattering coefficients of a human bladder wall [8, 9, 17, 29, 31, 32]. Moreover, the refractive index of titanium

dioxide and Intralipid is higher than that of silica particles and therefore more silica particles should be needed to achieve the same scattering coefficient as with titanium dioxide or Intralipid [30, 31]. To create the desired scattering coefficient by using microspheres as scattering agents multiple polymeric microspheres are needed of varying sizes. Extra research is necessary to determine the ratio in which the microspheres have to be mixed into the base material [28].

4.1.3. Phantom characteristics and fabrication process

The (bladder) phantoms described in literature differed with regard to characteristics and fabrication process. In this section relevant designs and methods used to develop these phantoms are addressed. Previous research has been done to create 3D bladder phantoms in which the three layers of the bladder wall are included [8, 17]. Another phantom does comply with the 3D shape of a human bladder except the three-layered structure [27]. Moreover, phantoms are described that include different layers, but do not comply to the anatomy of the bladder [9, 31]. In table 1 an overview is given of the relevant characteristics of the different phantoms and the techniques and methods used to create the phantoms. In addition to table 1 a picture or schematic drawing of each phantom found in the literature study is shown in figure 5.

4.1.3.1. Bladder phantoms including layers

For the bladder phantom created by K.L. Lurie et al. (2014), shown in figure 5A, first an inner and outer mould is 3D printed to be able to fabricate the thickest layer, muscularis propria, by the sandwich moulding technique [17]. The mould consists of an inner and outer part and is shaped as the upper or bottom half of a bladder. The material (scattering agents mixed into the base material) is poured at the bottom of the outer mould. A piece of foil is crumpled around the inner mould to create a texture that resembles the surface of each layer of a human bladder wall. Hereafter the inner mould is put into the outer mould and a wall is formed in between. The lamina propria is spin coated on top of the muscularis propria. The texture is applied again with the crumpled foil around the inner mould. To create tumour sites excisions of the cured layers are performed and these excised regions are filled with material that matches the optical properties of the tumour type. Subsequently, blood vessels are drawn on the surface of the lamina propria layer with a red permanent marker. The process of spin coating and applying texture is repeated on top of the lamina propria to create the urothelium layer. The upper and bottom half of the bladder phantom are created separately and bonded together at the end when also a tube representing the urethra is added.

G.T. Smith et al. (2016) created a bladder phantom by using a different technique [8]. This phantom is depicted in figure 5B. A mould including the entire surface of a bladder is 3D printed. The technique of air-brushing is used to spray coat the thinner layers. Texture is added to the inner surface of the phantom by covering the mould in crumpled foil before the urothelium layer is spray coated on top of the mould. Hereafter blood vessels are drawn on the urothelium by using a red permanent marker. The lamina propria layer is spray coated on top of the urothelium. To create the muscularis propria the sandwich moulding technique is used. The material is poured in the gap between the lamina propria and the outer mould. Once the muscularis propria layer has cured the outer mould and the inner mould on the inside of the urothelium layer are removed and a tube that represents the urethra is added. Tumour sites were included similarly to that of the phantom created by K.L. Lurie et al., namely by excisions of the cured layers and the addition of materials that match the optical properties of the different tumour types [17].

4.1.3.2. Bladder phantom without layers

The bladder phantom created by E. Choi et al. (2021) shown in figure 5C does not include the three layers of the bladder wall nor a textured surface [27]. Moreover, the already described technique of sandwich moulding with a 3D printed mould is used to create the phantom. However, the method of creating blood vessels and the inclusion of tumours differs from the already discussed phantoms. Therefore it is relevant to mention the fabrication of this phantom regarding these aspects. The blood vessels are created by using a negative inner mould. This mould contains grooves that represent the vascular structures of the bladder wall. The grooves are filled with red dyed material. After the layer of blood vessels is cured the actual layer of the bladder wall is added on top of the blood vessel layer. This results in a bladder phantom that includes a 3D vascular network on the inside surface of the phantom wall. The tumours included in this phantom are ellipsoidal papillary tumours that are positioned on the inner phantom wall. The tumour models contain a magnet. A magnet on the outside of the phantom can be used to reposition the tumour model to any desired place. This method makes it possible to use the phantom for diverse endoscopic training and biopsy simulations.

4.1.3.3. Phantoms without a bladder shape including layers

These phantoms do not have the shape of a bladder or include blood vessels as the phantoms that are already discussed, but the techniques used to create the three layers are relevant to address. G.T. Smith et al. (2014) created a phantom on a flat surface, as can be seen in figure 5D, by a technique named painting [9]. The surface is covered in crumpled foil to add texture whereafter a drop of material is put in the middle of the surface and a flexible rubber spatula is used to spread the material evenly to create the urothelium. A layer is painted on top of the urothelium to represent the lamina propria. A layer is crumpled foil is pressed into the lamina propria before it has cured to create texture. The phantom is put in a box and a thick layer of material is poured on the lamina propria to fabricate the muscularis propria. Different tumour types are included in the phantom by material excision and filling, similar to phantoms described in section 4.1.3.1.

D.M.M. de Bruin et al. (2010) fabricated a phantom by using the sandwich moulding technique [31]. A part of an image made of such a phantom is shown in figure 5E. Instead of using 3D printed moulds the phantom was created in between two glass plates. One plate can be modified to create grooves or other texture characteristics on the phantom layers. Subsequent layers can be moulded on top of previously cured layers to create a multi-layered phantom. No tumours were included in this phantom.

Table (1) *An overview is given of the characteristics of the different (bladder) phantoms found in the literature study and the techniques and methods used to fabricate these phantoms.*

Reference →	K.L. Lurie et al. (2014) [17]	G.T. Smith et al. (2016) [8]	E. Choi et al. (2021) [27]	G.T. Smith et al. (2014) [9]	D.M.M. de Bruin et al. (2010) [31]
Bladder shape	Yes	Yes	Yes	No	No
Three layers	Yes	Yes	No	Yes	Yes
Used technique(s)	Spin coating, sandwich moulding with 3D printed mould	Air-brushing, sandwich moulding with 3D printed mould	Sandwich moulding with 3D printed mould	Painting	Sandwich moulding with glass plates
Inclusion of tumours	Yes	Yes	Yes	Yes	No
Inclusion of blood vessels (and method)	Yes, drawn by red permanent marker	Yes, drawn by red permanent marker	Yes, negative inner mould	No	No
Inclusion of textured surface (and method)	Yes, textured by crumpled foil	Yes, textured by crumpled foil	No	Yes, textured by crumpled foil	Yes, textured by machined glass plate

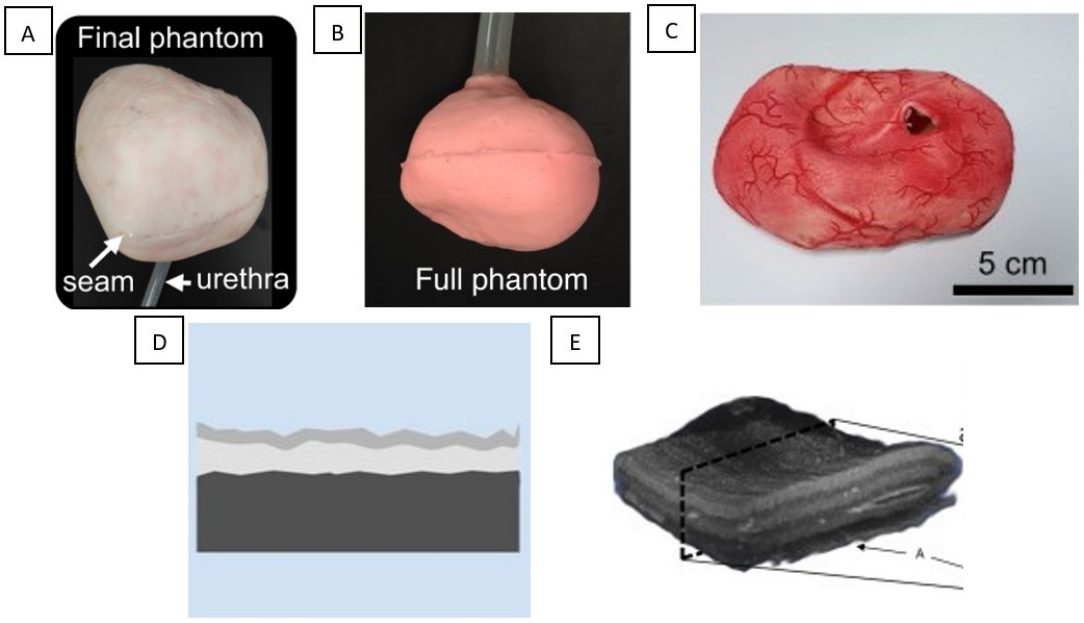

Figure (5) *Pictures or schematic drawings of the different (bladder) phantoms found in the literature study are shown. Some of the phantoms characteristics described in section 4.1.3 and in table 1 can be seen in these pictures and drawings. A) K.L. Lurie et al. (2014) [17]. B) G.T. Smith et al. (2016) [8]. C) E. Choi et al. (2021) [27]. D) G.T. Smith et al. (2014) [9]. E) D.M.M. de Bruin et al. (2010) [31].*

4.2. Requirements

Before the phantom can be designed the requirements, functional as well as technical, have to be determined. These requirements should comply with the interests of the stakeholders, RaM, Scinvivo and the University of Twente, namely the creation of an improved phantom with respect to the phantom that is now being used for experiments with the Next-Gen In-Vivo robot-controlled catheter.

4.2.1. Functional requirements

The functional requirements describe the functions the phantom should be able to carry out. The phantom should:

- represent the anatomy of a human bladder
- represent the physiology of a human bladder
- represent the pathology of a human bladder
- resemble the imaging results of a human bladder
- be suitable for experiments with the robot-controlled catheter that is developed for the Next-Gen In-Vivo project
- be suitable for easy fabrication

4.2.2. Technical requirements

The technical requirements describe the extent in which the phantom should comply with the functional requirements. In table 2 the technical requirements for the phantom are organised per functional requirement. For every technical requirement at least one specification is given that describes relevant (measurable) aspects for the actual design of the phantom. Some technical requirements are more important to focus on than others, this is addressed in the column Importance in table 2. A grade between 1 (least important) and 10 (most important) is given to every technical requirement. Technical requirements that are given a 5 or less in the Importance column in table 2 are labelled as a wish instead of a requirement. Although it would add value to the phantom if the specifications of these wishes would be met, it is not something to be focused on during the design of the phantom.

As can be concluded from the marks given in the Importance column in table 2 the most important requirements are about the inclusion and thickness of the three layers of the bladder wall in the phantom and the visibility of those layers by OCT and ultrasound. Also, the usability of the phantom for experiments performed with the robot-controlled catheter developed for the Next-Gen In-Vivo project is important. Besides, it is highly desired that the different types of bladder cancer are included and visible by OCT and ultrasound. Other focus points of the phantom are its shelf life and an easy and accessible fabrication process. The least important requirements are the texture, size and self-sufficiency of the phantom.

The most important wishes cover aspects of the phantom regarding its elasticity, visual resemblance to a human bladder wall including healthy and tumorous tissue and specific optical properties of the layers. Furthermore, wishes about the anatomical correctness of the phantom are described, namely the shape and inclusion of ureters, urethra and biological components in the layers of the phantoms wall such as blood vessels. Being able to fill and empty the phantom and store liquid in between is the least important wish.

Table (2) *The technical requirements and specifications for the creation of the phantom are organized per functional requirement. Every technical requirement has been given a score between 1 (least important) and 10 (most important) to rank the importance. A score of 5 or less denotes a wish rather than an actual requirement.*

Name	Technical requirement	Specification	Requirement or wish	Importance
Represent the anatomy of a human bladder				
R1	The phantom should represent the shape of a human bladder	The shape of an actual human bladder should be used for the design of the phantom	Wish	4
R2	The phantom should have the same size as a human bladder	The phantom of a complete bladder should be able to contain the same volume as the average capacity of a human bladder, namely 500 mL [4]	Requirement	6
R3	The phantom should include a representation of the ureters and urethra	Two tubes are attached to the lateral sides of the phantom to represent the ureters and one tube is attached on the caudal side of the phantom to represent the urethra [4]	Wish	4
R4	The inside surface of the phantom should represent the lining of the bladder wall	The texture of the inner surface of the phantom should be similar to that of the bladder wall [4]	Requirement	7
R5	The phantom should include the three bladder wall layers	The three layers should be distinguishable by imaging with OCT and ultrasound [4]	Requirement	9
R6	The thicknesses of the three layers in the phantom should comply to the ratio of these thicknesses in a human bladder wall	The ratio of 1 : 5 : 32 must comply for the thicknesses of the urothelium, lamina propria and muscularis propria respectively with a maximum error of 5% [8]	Requirement	8
R7	The phantom should include the biological components inside the tissue of the bladder wall.	The phantom should include blood vessels, nerves, fibroblast, etc. [4]	Wish	4
Represent the physiology of a human bladder				
R8	The phantom should represent the elasticity of a human bladder	The Young's modulus of the phantom should be around 284 kPa [33]	Wish	5
R9	It should be possible to fill the phantom with a liquid whereafter the liquid is stored in the phantom. It should also be possible to empty the phantom	The phantom should store 500 mL of liquids without leaking [4]. The liquid could conveniently be put into and removed from the phantom	Wish	3

Represent the pathology of a human bladder				
R10	The phantom should include the different bladder cancer types	Characteristics of the different tumour types should be recognizable by imaging with OCT and ultrasound [8, 20]	Requirement	8
R11	The phantom should include the visual characteristics of tumours in the bladder	Redness and thickening of the tumour sites should be visible on the inner surface of the phantom by imaging with the miniature camera [24-26]	Wish	5
Represent the imaging results of a human bladder				
R12	The layers of the phantom should be distinguishable when the phantom is imaged by OCT and ultrasound	The ratio of 1 : 4 : 3, based on the scattering coefficients per layer, must comply for the intensities of the urothelium, lamina propria and muscularis propria respectively with a maximum error of 5% when the phantom is imaged by OCT and ultrasound [8, 20]	Requirement	9
R13	The layers in the phantom represent perfectly the optical and acoustic characteristics of the layers in a human bladder wall when the phantom is imaged by OCT and ultrasound	The scattering coefficients of the layers in the phantom should be 0.49±0.25 mm^{-1}, 2.0±0.7 mm^{-1} and 1.38±0.7 mm^{-1} for the urothelium, lamina propria and muscularis propria respectively [8]	Wish	5
R14	It should be possible to evaluate the thickness of the layers of the phantom when the phantom is imaged by OCT and ultrasound	The ratio of 1 : 5 : 32 must comply for the thicknesses of the urothelium, lamina propria and muscularis propria respectively with a maximum error of 5% [8]	Requirement	9
R15	The inner surface of the phantom should resemble the surface of a human bladder wall when it is imaged by the miniature camera	The texture of a human bladder as is shown in literature should be recognizable when the inner surface of the phantom is imaged by the miniature camera [9]	Requirement	7
R16		Blood vessels as are shown in literature should be visible when the inner surface of the phantom is imaged by the miniature camera [24-26]	Wish	4
R17		Redness and thickening of the tumour sites as is shown in literature should be visible when the inner surface of the phantom is imaged by the miniature camera [24-26]	Wish	5

R18	Characteristics of the different tumour types should be recognizable by imaging with OCT and ultrasound	The OCT and ultrasound scans of the sites of the different tumour types in the phantom should represent OCT scans shown in literature made from a human bladder wall invaded by these tumour types [8]	Requirement	8
Be suitable for experiments with the robot-controlled catheter that is developed for the Next-Gen In-Vivo project				
R19	The phantom should be suitable for the evaluation of the imaging techniques used by catheter	The optical and visual characteristics of the human bladder wall should be included in the phantom to be able to do OCT and miniature camera tests	Requirement	9
R20	The catheter should be able to reach into the phantom	An opening of at least 3 cm in diameter should be included so the catheter can be inserted into the phantom to be able to perform experiments using the phantom	Requirement	9
R21	No support is needed when the phantom is used to perform experiments with	The phantom should be self-sufficient to stay in the same position while experiments are being performed with it	Requirement	6
R22	The phantom must have a shelf life of at least 3 years	The phantom must be strong enough so performing experiments with it for at least 3 years does not cause any damage to the phantom	Requirement	8
R23		The optical and visual properties of the phantom must be stable after fabrication for at least 3 years	Requirement	8
Be suitable for easy fabrication				
R24	It should not take a long time to fabricate the phantom	A maximum of 6 hours should be needed for fabricating the phantom, excluding the curing time	Requirement	8
R25	The phantom should be made of materials that are easily accessible	The materials used to fabricate the phantom should already be present at RaM or can easily be ordered online	Requirement	8
R26	The phantom should be fabricated with the help of techniques that are easily accessible	The materials and devices needed for the fabrication technique of the phantom should already be present at RaM or can easily be built or ordered online	Requirement	8

4.3. Phantom design

In the development process multiple choices were made based on the literature study and the requirements. The decisions made about the design of the phantom are explained in this section. Moreover, it is determined if this phantom design would comply with each of the requirements and wishes described in section 4.2 or not. To make it easier to navigate to certain aspects of the phantom design, the section is split into the subsections base materials, scattering agents, layers, shape and size, fabrication process and tumour sites.

4.3.1. Base materials

It has been decided to test out three base materials, namely Dragon Skin, Ecoflex and plastisol. The curing times of these materials will differ from a couple of minutes (plastisol), 75 minutes (Dragon Skin) to 4 hours (Ecoflex). The curing process is similar for Dragon Skin and Ecoflex, but very different from that of plastisol. Therefore, the effect of curing time and process can be researched. Moreover, the elasticity of these materials differ. The elasticity of Dragon Skin and plastisol should be similar to that of a human bladder while Ecoflex is less elastic than those materials [8, 27, 32, 33]. By choosing these materials it is possible to comply with wish R8. Furthermore, phantoms made of these materials should be strong and stable enough to comply with requirements R22 and R23 and a shelf-life of years should be reached [8, 27, 32]. Lastly, Dragon Skin, Ecoflex and plastisol can easily be ordered online worldwide so this is in accordance with requirement R25.

4.3.2. Scattering agents

The scattering agents that will be used are titanium dioxide and silica. These materials are both easily accessible (requirement R25) by ordering it online. The other scattering agents used in literature were less suitable since it would take more time to investigate the ratio for the polymeric microspheres and Intralipid has a similar refractive index as titanium dioxide but a lot more is known about titanium dioxide concentrations to achieve the desired scattering coefficients. By choosing titanium and silica the effect of different refractive indices can be researched.

4.3.3. Layers

The different layers are fabricated by adding different concentrations of scattering agents to each layer. This complies with requirements R5 and R19, since the layers will have different scattering coefficients and therefore appear with different intensities when the phantom is imaged by OCT and ultrasound. This also results in the ability to evaluate the thickness of the different layers by OCT and ultrasound (requirement R14). In section 5 it is described what concentrations of scattering agents have been tested for each layer. By testing multiple concentrations the correct concentrations can be determined to optimally distinguish layers in accordance with requirement R12. When the exact concentrations have been found so the phantom layers match the scattering coefficients of the urothelium, lamina propria and muscularis propria of a human bladder, wish R13 has been achieved.

4.3.4. Shape and size

To simplify the development of the phantom (requirements R24 and R26) it has been decided that the phantom does not have to resemble the shape of the bladder (wish R1). It will take the shape of a hemispherical wall. This can be seen as a simplified version of an upper or bottom part of a hollow bladder. An advantage of the hemispherical wall is that the opening of the hemisphere will be more than big enough, as per requirement R20, for the robot-controlled catheter to reach into

the phantom. Moreover, the hemispherical wall should be able to contain 250 mL, half the capacity of an average human bladder, to comply with requirement R2. No tubes will be attached to the phantom and therefore the specifications of wishes R3 and R9 will not be achieved. However, the phantom is in line with requirement R21, since the hemispherical wall should be able to remain in its position without support once it is placed somewhere.

4.3.5. Fabrication process

The choice of fabrication process is mainly focussed on complying with requirements R24 and R26. Techniques used in previous research like spin and spray coating require relatively complex spinning and air-brushing devices. Therefore, using these techniques would not comply with requirement R26. Moreover, the painting and sandwich moulding between glass plates techniques cannot be used for creating a hemispherical shaped phantom. The only technique that is left is sandwich moulding with a 3D printed mould. However, only thick layers are fabricated by this technique. For this reason another fabrication process must be applied where already used methods are combined with new methods. This fabrication process includes 3D printing an inner and outer mould to create the hemispherical wall in the gap between these moulds, just as is done by K.L. Lurie et al. (2014) [17]. Also, the inner mould is covered in crumpled foil, but instead of only wrapping one layer of aluminium foil around the inner mould to create texture, multiple layers of aluminium foil are used to cover the inner mould. This results in the thickening of the inner mould. Once the outer layer, muscularis propria, has been made a couple of layers of aluminium foil are removed so a space appears between the cured muscularis propria and the inner mould. The thickness of this space depends on the amount of aluminium foil layers that has been removed. For the creation of the urothelium only one layer of crumpled aluminium foil should be left on the inner mould. This means that the thickness of the layers can be adjusted in steps of the thickness of one layer of aluminium foil, which is around 20 µm, so the desired thickness ratio can be achieved in accordance to requirement R6. Also, the use of crumpled foil for each layer adds texture (requirements R4, R15 and partly R19). In conclusion, the described fabrication process is fast, easy and only aluminium foil and a 3D printer is needed. Therefore, this fabrication method complies with requirements R24 and R26. The only disadvantage is that the visual representation of the human bladder wall is not included in the fabrication process. No components like blood vessels and nerves are included, except for the three-layered structure, so the phantom design does not comply with wishes R7, R16 and partly requirement R19.

4.3.6. Tumour sites

Another compromise that has been made to simplify the development of the phantom (requirements R24 and R26) is that it has been decided to not include the tumour sites into the phantom, but to fabricate separate tumour test pieces. These tumour test pieces do not have a bladder shape, but do contain the three-layered structure. The fabrication method of these tumour sites are in accordance to the method used to create the tumour sites in the phantom made by G.T. Smith et al. (2014) [9]. This method complies with requirements R10 and R18, but not with wishes R11 and R17. This is because the visual characteristics of a bladder tumour like redness and thickening of the bladder wall are not included, since this was not the focus point for the creation of this phantom.

5. Materials and Methods

First, the specifics of the used materials and scattering agents are described. Then, for the development of the bladder phantom a mould had to be designed that complies with the decisions made in section 4.3. Once the mould was 3D printed phantoms could be made. However, before that test pieces were created to examine the properties of the materials and scattering agents. Moreover, test pieces were produced that include the representations of different tumour types. An overview of the created test pieces and phantoms is given. This table shows the different combinations of materials, scattering agents and scattering agent concentrations per layer. After the test pieces and phantoms were fabricated OCT scans, ultrasound scans and camera recordings were done that can be used for the evaluation discussed in the results section 6.

5.1. Used materials and scattering agents

As already addressed in section 4.3 three materials were tested for the phantom, namely Dragon Skin, Ecoflex and plastisol. The type of Dragon Skin that was used is Dragon Skin™ 10 Fast (Smooth-On). For Ecoflex the Ecoflex™ 00-30 (Smooth-On) was used. The plastisol that was used is plastisol Soft (Bricoleurre). Also, in section 4.3 the decision for the types of scattering agents is made: titanium dioxide and silica. The type of titanium dioxide that was used is Titanium(IV) oxide, anatase (Sigma-Aldrich). For silica a Silica gel 60 – 200 µm (VWR Chemicals) was used.

5.2. Mould design and 3D printing

To be able to make the bladder phantom a mould was designed, see figure 6. This mould consists of an outer and an inner part, both hollow hemispheres, that can be put into each other. In between these parts the materials can be poured to create the phantoms representation of the bladder wall once the materials have hardened.

For the design of the mould a bladder capacity of 500 mL was assumed [4]. Therefore the volume of the inner hemisphere of the phantom should be 250 mL. To achieve this volume it was calculated that the outer radius of the inner part of the mould should be approximately 50 mm. This radius is rounded up to an integer for convenience. For enough stability and strength the thickness of the walls of the mould was set to 8 mm. Therefore, the inner radius of the inner part of the mould is 42 mm.

The total thickness of an average human bladder wall is 1.9 mm, with a thinnest layer of 50 µm [8]. It is possible to create layers in the millimetre scale by using the chosen production method described in section 4.3.5, but it will be hard to create layers with thicknesses in the micrometre scale. Besides, the phantom would not be strong if the actual thickness of a human bladder wall would be realized. Therefore, it was decided to set the thickness of the phantoms wall to 8 mm. Consequently, the distance between the inner and outer part of the mould should be 8 mm. This means that the inner radius of the outer part of the mould should be 58 mm and the outer radius 66 mm. It should be possible to create a phantom wall with a total thickness of only a couple of millimetres by using the described fabrication process. However, a wall thickness of 8 mm is chosen to guarantee the strength of the phantom. Furthermore, by increasing the thicknesses it is easier to make the layers distinguishable, because the transition between larger intensity regions is spotted more easily and suffers less from noise than when very thin layers alternate in intensities.

If the mould would only consist of two hemispheres it would not be able to stand on a table while the materials are being poured in. That is why a cross of supportive walls was added underneath the hemisphere of the outer part of the mould. Also, a construction was made so the two cross-sectioned surfaces of the hemispheres are aligned to sustain the gap of 8 mm between the two mould parts all around the hemisphere. To achieve this an extra circular layer was added on top of the cross-sectioned parts of the hemispheres. Four extensions of this layer on the inner hemisphere were made to fit into four cutouts of the extra layer on the outer hemisphere. This way the top of the inner hemisphere rests on the top of the outer hemisphere. Moreover, the solid extra circular layer on top of the inner hemisphere can be used to put pressure on the inner part of the mould to push the material upwards between the mould parts.

The mould parts were modelled in SolidWorks with the dimensions and features as discussed earlier in this section. Images of this model are depicted in figure 6. The SolidWorks model was converted to a STL file and opened in Ultimaker Cura 4.3.0 to prepare for 3D printing. The mould parts were 3D printed in an Ultimaker S5 with a glass build plate of 60°C. White Tough PLA was used as the material with a print core of AA 0.4. The layer height was set at 150 µm and infill at 10%. The number of perimeters was set at 4 which means that the perimeter of a 3D printed layer has a massive thickness of 1.6 mm and the part of the layer within the perimeter is only partially filled, namely for 10%. Gradual infill and adhesion were turned off. For support Extruder 1 was chosen. After 1 day, 20 hours and 27 minutes the 3D printed mould was finished and could be used to fabricate phantoms. In figure 7 pictures of the 3D printed mould are shown.

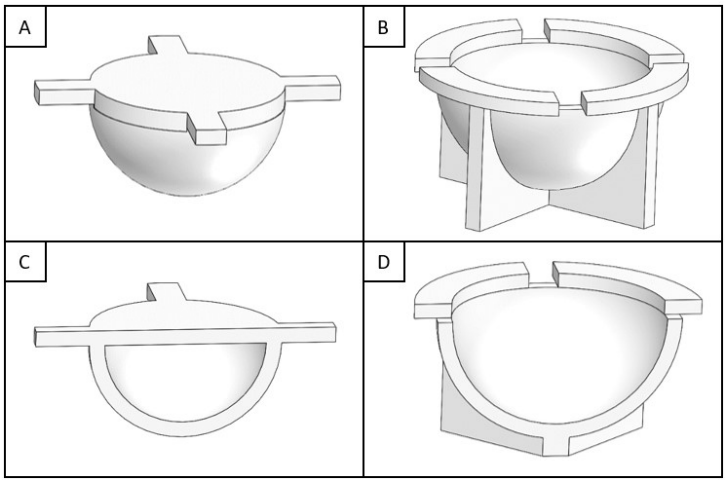

Figure (6) *The mould used for the fabrication of the bladder phantom is modelled in SolidWorks. A) Inner part of the mould. B) Outer part of the mould. C) Cross-section of the inner part of the mould. D) Cross-section of the outer part of the mould.*

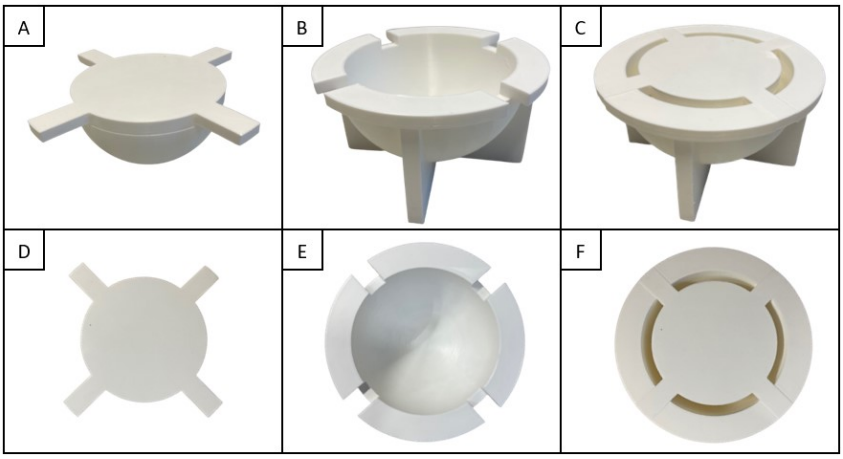

Figure (7) *Pictures of the 3D printed mould used for the fabrication of the bladder phantom. A) Inner part of the mould. B) Outer part of the mould. C) Inner part inside the outer part of the mould. D) Top view of the inner part of the mould. E) Top view of the outer part of the mould. F) Top view of the inner part inside the outer part of the mould.*

5.3. Test pieces

For the fabrication of test pieces the mould was not used. Instead, the materials were poured in plastic containers of various sizes. The purpose of the creation of test pieces is to be able to examine the different materials and scattering agents in different concentrations before a phantom was made by using the mould. In the following sections the reasoning behind the chosen layer thicknesses and the fabrication process of the test pieces are described.

5.3.1. Layer thickness

To obtain the necessary amounts of materials per plastic container the surface of the container was determined whereafter this was multiplied by the desired thickness of the different layers of the bladder wall phantom. The thickness of the layers of a healthy human bladder wall are 50 µm, 250 µm and 1.6 mm for the urothelium, lamina propria and muscularis propria respectively [8]. As it is not possible to achieve such thin layers as already discussed in section 5.2 it is chosen to create layers of 2 mm, 2 mm and 4 mm for the urothelium, lamina propria and muscularis propria respectively. Hereby the total thickness of the test pieces is equal to the thickness of the phantoms, since the distance between the outer and inner part of the phantom mould is 8 mm as stated in section 5.2. Moreover, by choosing these thicknesses it is possible to observe the difference in thickness between the two thinner layers, urothelium and lamina propria, and the significant thicker muscularis propria.

5.3.2. Fabrication process

The method of fabrication of the test pieces differed per material. Therefore, the process of creating the test pieces will be discussed separately for every used material.

5.3.2.1. Dragon Skin

For preparing the Dragon Skin the instructions of the manufacturer were followed. In short, Part A and B were stirred thoroughly in their separate containers whereafter the two parts were poured in a beaker in a 1:1 ratio by weight to get the total desired weight of material. The desired amount of scattering agent was added after which all the substances were mixed together. The pot life of

the used Dragon Skin is only 8 minutes so the mixture was poured in the plastic container to create the test piece in after only a few minutes of stirring. When the surface of the plastic container was covered it was put in a vacuum machine until no more air bubbles were seen in the mixture. The Dragon Skin had to cure for at least 75 minutes before adding a new layer by repeating the described process.

5.3.2.2. Ecoflex

The same method for Dragon Skin was applied for Ecoflex until all the substances were mixed together. The pot life of Ecoflex is 45 minutes which means that the air bubbles inside the mixture can be removed before the material was poured in the plastic container to create the test piece in. After no more air bubbles were observed the mixture was taken out of the vacuum machine and carefully poured in the plastic container. After the mixture had cured for at least 4 hours this process was repeated to create more layers.

5.3.2.3. Plastisol

The desired amount of plastisol was poured in a heat-resistant container after which it was put in the vacuum machine until no more air bubbles were observed in the plastisol. Subsequently, the heat-resistant container was placed on a heating device set at 240°C that heated the plastisol until the white liquid appeared transparent. Thereafter the desired amount of scattering agent was mixed into the plastisol. Once the scattering agent was evenly distributed into the liquid it was poured in the plastic container to create the test piece in. The process was repeated to create multiple layers. This was done after the mixture was cooled down in the plastic container.

5.4. Phantoms

For the fabrication of the phantoms, the mould described in section 5.2 was used. The chosen method to create the various layers of the phantoms is already described in section 4.3.5. So instead of pouring a new layer on top of the cured previous layer(s) as is done for the test pieces described in section 5.3.2 different amounts of layers of aluminium foil are used for the creation of a thick muscularis propria and thinner lamina propria and urothelium in the phantoms. This process is depicted in figure 8. The aluminium foil was wrapped tightly layer per layer around the hemisphere of the inner part of the mould. Parts of the aluminium foil that covered the four extensions of the inner part of the mould were cut out. Furthermore, the pieces of aluminium foil between the four extensions were shortened and wrapped around the top of hemisphere onto the flat surface of the inner part of the mould. This secured the aluminium foil wrap. For the creation of the muscularis propria 10 layers of aluminium foil were wrapped around the inner part of the mould. For the lamina propria this was 5 layers and for the urothelium only one layer of aluminium foil was used. In the Results section 6 the actual thicknesses of the created phantom layers are evaluated when these numbers of aluminium foil layers are used.

Except for the difference in method to create layers the fabrication process of the phantoms is similar to that of the test pieces. Therefore, the steps described in section 5.3.2 were followed for the creation of the phantoms made of the different materials, namely Dragon Skin, Ecoflex and plastisol. However, in the case of the phantoms the mixtures were not poured in a plastic container but at the bottom of the outer part of the mould. Hereafter the inner part of the mould wrapped in (several layers of) aluminium foil was pushed into the outer part of the mould. Consequently, the mixture at the bottom of the outer part of the mould was pushed up along the sides to fill up the whole gap between the outer and inner parts of the mould. Once the mixture had cured a

hemispherical wall was created. For the creation of a successive layer the previously made layer(s) was or were not removed from the outer part of the mould. The mixture for the new layer was poured at the bottom of the previous layer(s) in the outer part of the mould whereafter the fabrication process was repeated.

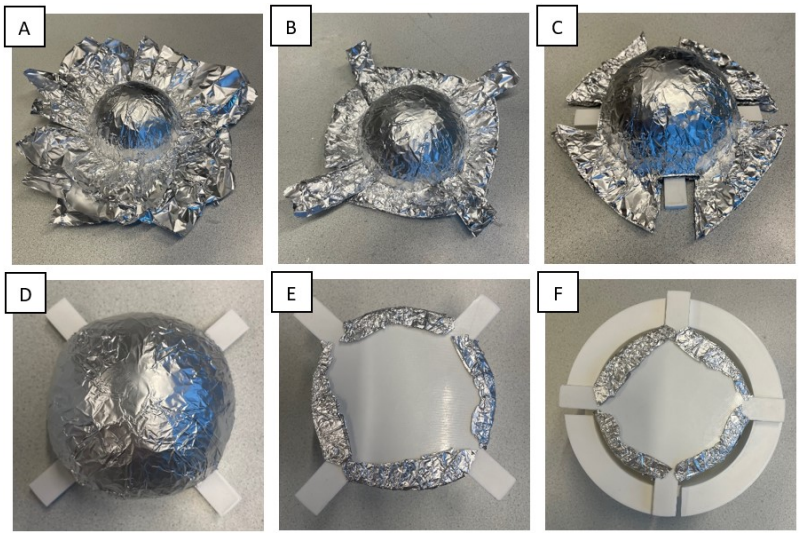

Figure (8) *Pictures are shown of the different steps performed regarding a new method to create relatively thin layers while using the sandwich moulding technique. The total thickness of the aluminium foil layers that are removed before creating the next phantom layer is the same as the thickness of the layer that is being created next. A) The inner part of the mould is wrapped tightly layer by layer in aluminium foil. B) The parts of the aluminium foil between the four extensions of the inner part of the mould are shortened. C) The parts of the aluminium foil that cover the four extensions are cut out. D) The parts of the aluminium foil between the four extensions are wrapped around the edge of the inner part of the mould. E) The aluminium foil layers are tightly secured around the inner part of the mould. F) The gap between the inner and outer part of the mould is reduced by the desired thickness dependent on the number of aluminium foil layers.*

5.5. Tumour test pieces

In section 2.2 four types of bladder cancer are described. To represent these tumour types tumour test pieces were created. Each tumour test piece included a pair of replicates of two different tumour types. In section 3.1 in figure 2 the OCT scans of the tumour types in a human bladder are depicted. Schematic drawings were made that represent the simplified versions of these OCT scans. The drawings are shown in figure 9. The darker the drawn layer, the darker it should appear in an OCT scan. The schematic representations of the tumours function as a guideline for the creation of the tumour test pieces in which the simplified versions of the different tumour types should be seen by OCT. The fabrication process of the tumour test pieces will be discussed per tumour type.

5.5.1. Urothelial dysplasia

To fabricate a representation of urothelial dysplasia (figure 9B) first a regular layer of urothelium is created. After this layer is cured a washer with a desired inner diameter for the tumour was placed on top of the urothelium layer and another urothelium mixture was poured into the washer until a thickening of 1 mm was achieved. After the thickening of the urothelium had cured the washer was removed and the lamina propria and muscularis propria layers were created.

5.5.2. Carcinoma in situ (CIS)

To create the CIS tumour as depicted in figure 9C first the urothelium and lamina propria layers of the tumour test piece were created. Hereafter, at the tumour site the two layers were removed with the desired diameter of the tumour. This hole was filled with a lamina propria mixture, the mixture with the highest intensity, until the surface of the previously created lamina propria layer was reached. After the filling was cured the muscularis propria layer was fabricated.

5.5.3. T1

Just as with the creation of the CIS tumour for the fabrication of the T1 tumour (figure 9D) the urothelium and lamina propria layer were created and removed with the desired tumour diameter. Subsequently, mixtures were formed for the lamina propria (highest intensity) and muscularis propria layer (low intensity). The hole was half-filled with the lamina propria mixture followed directly by filling it up with the muscularis propria mixture until the surface of the previously created lamina propria layer was reached. Since the mixtures did not have the time to cure yet, the filling could be stirred carefully so the two mixtures mix a bit and a transition zone between the two mixtures is created. After the filling had cured the muscularis propria layer was fabricated.

5.5.4. T2

All the three layers were created in the tumour test piece container, urothelium, lamina propria and muscularis propria before the T2 tumour in figure 9E can be formed. After these layers had cured the three layers were removed at the tumour site with the desired diameter of the tumour. This hole was filled and carefully stirred as was done for the creation of the T1 tumour. However, now the hole is three layers high and filled for one-third with the highest intensity lamina propria mixture and two-third with the low intensity muscularis propria mixture. After the curing of the filling no more layers were added.

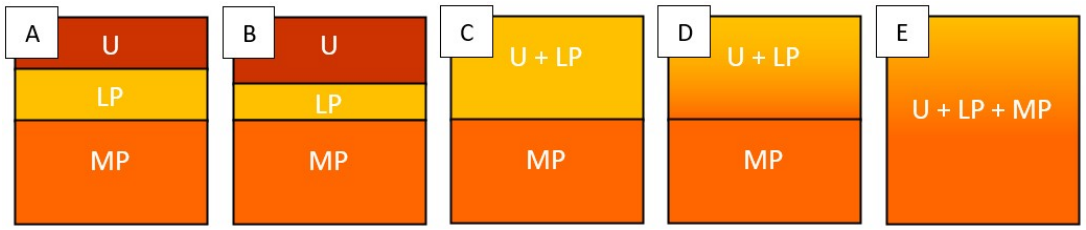

Figure (9) *Schematic representation of healthy bladder wall layers and different bladder cancer tumour types. The darkness of the colours represents the intensity on an OCT image. The abbreviations (U, LP, MP) indicate in what area the layers are represented. U: urothelium. LP: lamina propria. MP: muscularis propria. A) Healthy, clearly demarcated layers. B) Urothelial dysplasia, thickened U. C) Carcinoma in situ (CIS), fused U and LP with a clear demarcation with MP. D) T1, fused U and LP without a clear demarcation with MP. E) T2, no clear demarcation between layers.*

5.6. Created test pieces and phantoms

Eventually 19 test pieces, 5 phantoms and 6 tumour test pieces were created. These all differed in type of material and scattering agent and in the concentrations of the scattering agents mixed into the separate layers. An overview of the created test pieces and phantoms is shown in table 3. Different amounts of scattering agents were mixed into the materials to test the effect of scattering agent concentration on the visibility of the different layers in the phantoms for the different imaging

techniques. The scattering agent concentrations were measured as weight by weight percentages (% w/w). For Dragon Skin mixed with titanium dioxide previous research has shown that weight by weight percentages of 0.05, 0.2 and 0.1 % w/w would comply with the exact scattering coefficients of the urothelium, lamina propria and muscularis of the human bladder respectively [8]. Besides these weight by weight percentages multiple other combinations of weight by weight percentages for the urothelium, lamina propria and muscularis propria layers were tested for the different materials and scattering agents as is shown in table 3. Some tumour test pieces and phantoms only consist of one or two layers, as is indicated by "n.a." in table 3 for the layers that were not created. The three-layered structure was not finished since the ultrasound scans that were made after the first or second layer was created showed that the fabrication process or use of materials had to be adapted to achieve the desired result so it was unnecessary to finish these tumour test pieces and phantom.

Table (3) *An overview is given for the created test pieces and phantoms. The table shows the combinations of the weight by weight percentages (% w/w) of the scattering agents (titanium dioxide and silica) mixed into the materials (Dragon Skin, Ecoflex and plastisol) per layer of the test pieces and phantoms. Per group (test pieces, phantoms and tumour test pieces) the order in which it is shown in the table is the same as the order of fabrication. U: urothelium. LP: lamina propria. MP: muscularis propria. n.a.: not applicable.*

Name	Material	Scattering agent	U (% w/w)	LP (% w/w)	MP (% w/w)
Test pieces					
DT1	Dragon Skin	Titanium dioxide	0.05	0.2	0.1
DT2	Dragon Skin	Titanium dioxide	0.05	0.2	0.1
DT3	Dragon Skin	Titanium dioxide	0.05	0.3	0.1
DT4	Dragon Skin	Titanium dioxide	0.1	0.4	0.2
DS1	Dragon Skin	Silica	0.1	0.4	0.2
DT5	Dragon Skin	Titanium dioxide	0.05	0.2	0.1
DT6	Dragon Skin	Titanium dioxide	0.05	0.2	0.1
PT1	Plastisol	Titanium dioxide	0.25	1	0.5
PS2	Plastisol	Silica	0.5	2	1
PS3	Plastisol	Silica	0.2	3	1
PS4	Plastisol	Silica	0.2	3	1
ES1	Ecoflex	Silica	0.2	3	0.4
ES2	Ecoflex	Silica	0.1	1.5	0.2
ET2	Ecoflex	Titanium dioxide	0.2	3	0.4
DS2	Dragon Skin	Silica	0.2	3	0.4
DS3	Dragon Skin	Silica	0.1	1.5	0.2
DT10	Dragon Skin	Titanium dioxide	0.2	3	0.4
PS5	Plastisol	Silica	0.2	3	0.4
PS6	Plastisol	Silica	0.2	3	0.4
Phantoms					
PS1	Plastisol	Silica	unknown	unknown	unknown
DT9	Dragon Skin	Titanium dioxide	n.a.	n.a.	0.1
ET1	Ecoflex	Titanium dioxide	0.05	0.2	0.1
ES3	Ecoflex	Silica	0.2	3	0.4
PS11	Plastisol	Silica	0.2	3	0.4
Tumour test pieces					
DT7	Dragon Skin	Titanium dioxide	0.05	0.2	n.a.
DT8	Dragon Skin	Titanium dioxide	0.05	0.2	n.a.
PS7	Plastisol	Silica	0.2	3	0.4
PS8	Plastisol	Silica	0.2	3	n.a.
PS9	Plastisol	Silica	0.2	3	0.4
PS10	Plastisol	Silica	0.2	3	0.4

5.7. OCT scans

The OCT scans were performed on an OCT scanning device fabricated by Scinvivo. The test setup is shown in figure 10. The OCT probe integrated in this device is the same as could be used for the robot-controlled catheter developed for the Next-Gen In-Vivo project. To scan the test pieces, phantoms and tumour test pieces, hereafter named samples, were placed under the OCT probe. The distance between the samples and the OCT probe was determined by decreasing this distance until the surface of the sample was seen almost at the top of the OCT image. Even though OCT scanning moments were limited, an adequate number of samples has been scanned to be able to draw conclusions from the OCT images. The settings of the software for the OCT scanning device are shown in table 4. It is important to note that per sample a surface of 4 by 5 mm was scanned into the depth. This is done by scanning a 5 mm line in depth until the penetration depth has reached to image a cross-section of the sample. Per scanned sample 41 cross-sections were imaged with steps of 0.1 mm. Thereby a 3D OCT image could be generated. The scans were made in the middle of the sample or at an interesting part of the sample, for instance at an indentation where an air bubble used to be to see the surface structure or at a tumour site to see if the tumorous characteristics are visible.

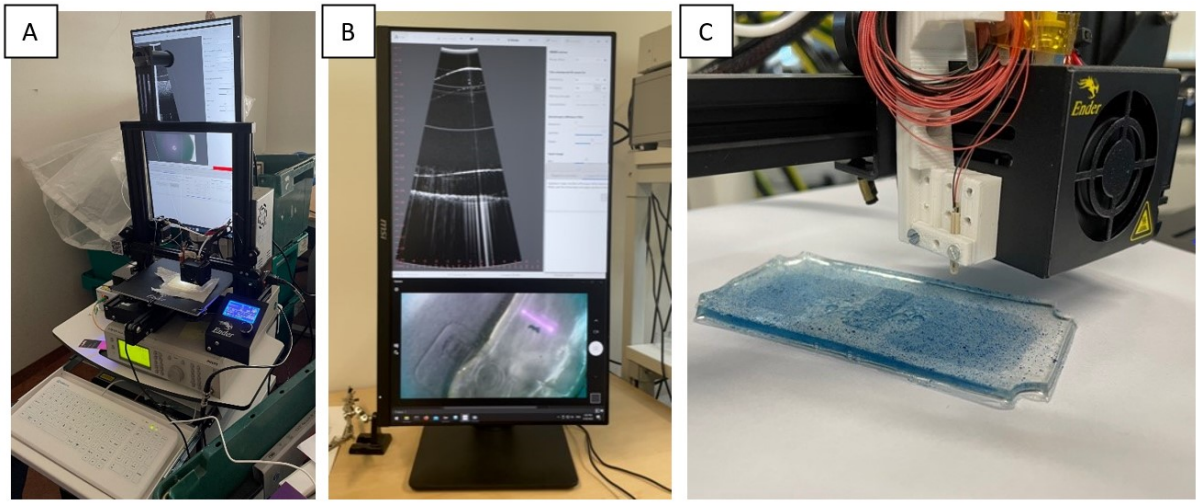

Figure (10) *Pictures of the test setup for imaging by OCT are shown. The OCT setup is constructed by Scinvivo from a 3D printer installation. A) The total setup is shown. The samples are placed on a table that can move in two directions to bring the sample in the right position for the OCT scan. Also the box where normally the material used for 3D printing comes out of can move. This is where the OCT probe is attached so it enables the scanning in every direction. B) The monitor displays the real-time OCT image, the real-time recordings made by a miniature camera of the spot on the sample that is being scanned and the settings. C) A close-up of the OCT probe is shown. It is secured in a holder connected to the 3D printer construction. This part of the 3D-printer, and thereby the OCT probe, is able to move in all three direction.*

Table (4) *The settings of the software for the OCT scanning device when OCT scans were made of the test pieces, phantoms and tumour test pieces are shown in this table. For every sample (test piece, phantom or tumour test piece) a scan of in total 4 mm was made in steps of 0.1 mm to create a 3D OCT image.*

Setting	Value
MEMS mirror	
Phase offset	27
Use subsequent B-scans for	
Interlacing	2x
Averaging	4x
Moving average	Off
Consolidation	Accurately located
Anisotropic diffusion filter	
Iterations	0
Lambda	0.25
Kappa	30
Input Range	
Min.	-20
Max.	-6

Setting	Value
Plot	
Coordinate system	Polar
Interpolation	Scinvivo
C-scan steps	
Steps	40
Pitch	0.100 mm
Angle	110.0°
Settling time	100 ms
Perpendicular steps	
Steps	0
Pitch	5.000 mm

5.8. Ultrasound scans

The ultrasound device that was used to create the ultrasound images is a Siemens ACUSON X300 with a VF13-5 transducer. The settings of the ultrasound device are shown in table 5. The samples were placed on a flat surface. A bit of Aquasonic ultrasound transmission gel was put on the scanning part of the transducer and the transducer was lightly pressured onto the surface of the sample. For the test pieces one horizontal and one vertical (when the sample is viewed from above) scan was made in the middle of the test piece, both from the top and the bottom surface of the sample. Besides these four images, a recording sequence was performed which resulted in a clip in which the sample has been scanned from the top surface of the sample from one side to the other side. For the phantoms multiple scans were made both from the in and outside and from the top and bottom parts. Also, recording sequences were performed where the transducer moved from the top of the hemisphere towards the bottom. For the tumour test pieces, images were made when the transducer was put horizontally and vertically on the regular, healthy part in the middle of the test piece both from the top and bottom surface of the test piece. Moreover, for the tumour sites images were made while the transducer crossed the tumour site as well as regular, healthy parts of the tumour test piece. Per tumour site scans were made while the transducer crossed the tumour horizontally as well as vertically and both from the top and bottom surface of the tumour test piece.

Table (5) *The settings of the ultrasound device when the ultrasound scans were made of the test pieces, phantoms and tumour test pieces are shown in this table.*

Setting	Value
MultiHertz	8.9 MHz
DR	65 dB
Edge	1
Persist	3
R/S	4
Map	C

Setting	Value
Tint	1
SieClear	2
DTCE	Low
Frames per second	26
Depth	3 cm
Focus	0.5 cm

5.9. Camera recordings

The camera recordings were made by the Ultra Mini CMOS Color Camera type FXD-VB20903I-76 (Misumi Electronics Corporation, Taiwan). The image quality is derived from the resolution of 1280x720 pixels. The camera housing dimensions are 3.8 mm in diameter and 12 mm in length. This sort of camera can also be used for the robot-controlled catheter developed for the Next-Gen In-Vivo project. The camera was connected to a laptop by a USB cable. To visualise the view of the camera and to take images and videos the Camera App on the laptop was used. The images and videos were made with the light of the mini camera set to the highest brightness. For every phantom images were made at different spots of the phantom, at the top as well as at the bottom parts. Moreover, a video was taken for each phantom. The video was started at the top of the phantom after which the camera was moved along the phantoms wall in a circular motion spiralling down towards the bottom. The images and videos showed how the texture of the inner surface of the phantoms was displayed by the miniature camera.

6. Results

The scans made by the different imaging techniques performed on the test pieces, phantoms and tumour test pieces are shown and discussed. The test pieces, phantoms and tumour test pieces are evaluated by using these scans.

6.1. Test pieces

A picture of the 19 created test pieces is shown in figure 11. To the evaluate the test pieces OCT and ultrasound scans have been made as described in section 5. By analysing these scans the distinguishability between the different layers in the test pieces will be determined. First the results of the OCT scans will be discussed followed by the results of the ultrasound scans.

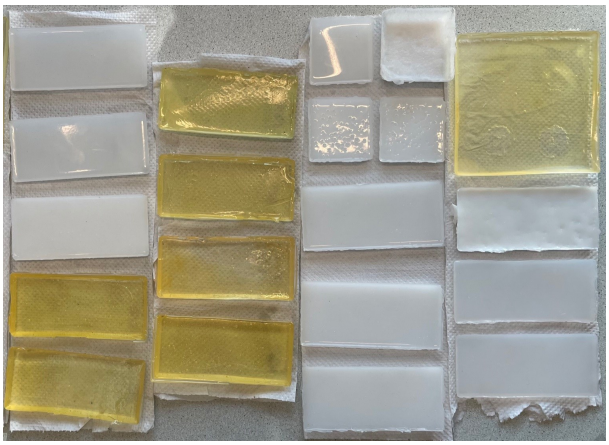

Figure (11) *Picture of the 19 test pieces (and one tumour test piece at the top right). The white coloured test pieces are made of Dragon Skin or Ecoflex and the yellow coloured test pieces are made of plastisol. The combination of concentrations of silica or titanium dioxide added per layer differs per test piece.*

6.1.1. OCT

For every base material and scattering agent combination an OCT scan has been selected. Each different base material and scattering agent combination will be called a condition. The conditions and the corresponding test pieces are shown in table 6. The weight by weight percentages of the scattering agents mixed into the base material are 0.2, 3 and 0.4 % w/w for the urothelium, lamina propria and muscularis propria respectively for every condition test piece, except for PT1. The weight by weight percentages used for the fabrication of PT1 are 0.25, 1 and 0.5 % w/w for the urothelium, lamina propria and muscularis propria respectively. A test piece with a different combination of weight by weight percentages is chosen for the plastisol-titanium dioxide condition, since PT1 is the only test piece that has been fabricated for this condition.

Table (6) *Every different combination of base material and scattering agent is called a condition. Per condition a test piece has been selected as shown in this table.*

	Dragon Skin	Ecoflex	Plastisol
Titanium dioxide	DT10	ET2	PT1
Silica	DS2	ES1	PS6

When the test pieces were imaged by OCT no three-layered structure was seen for any of the test pieces. A couple of OCT images made of the test pieces are shown in figure 12. The bright (white) line at around -13 mm in Z-direction represents the top surface of the test piece. The part of the OCT scan under this line is the image of the cross-section of the test piece. No alternating regions of low, high and low intensity are visible as would be expected for the three-layered structure. Instead the OCT scans show a light grey image where the intensity transitions to a lower intensity at the bottom. The OCT scans of the test pieces that contain titanium dioxide as a scattering agent show high intensity spots in the image of the cross-section of the test pieces, while the test pieces that contain silica do not show those white spots.

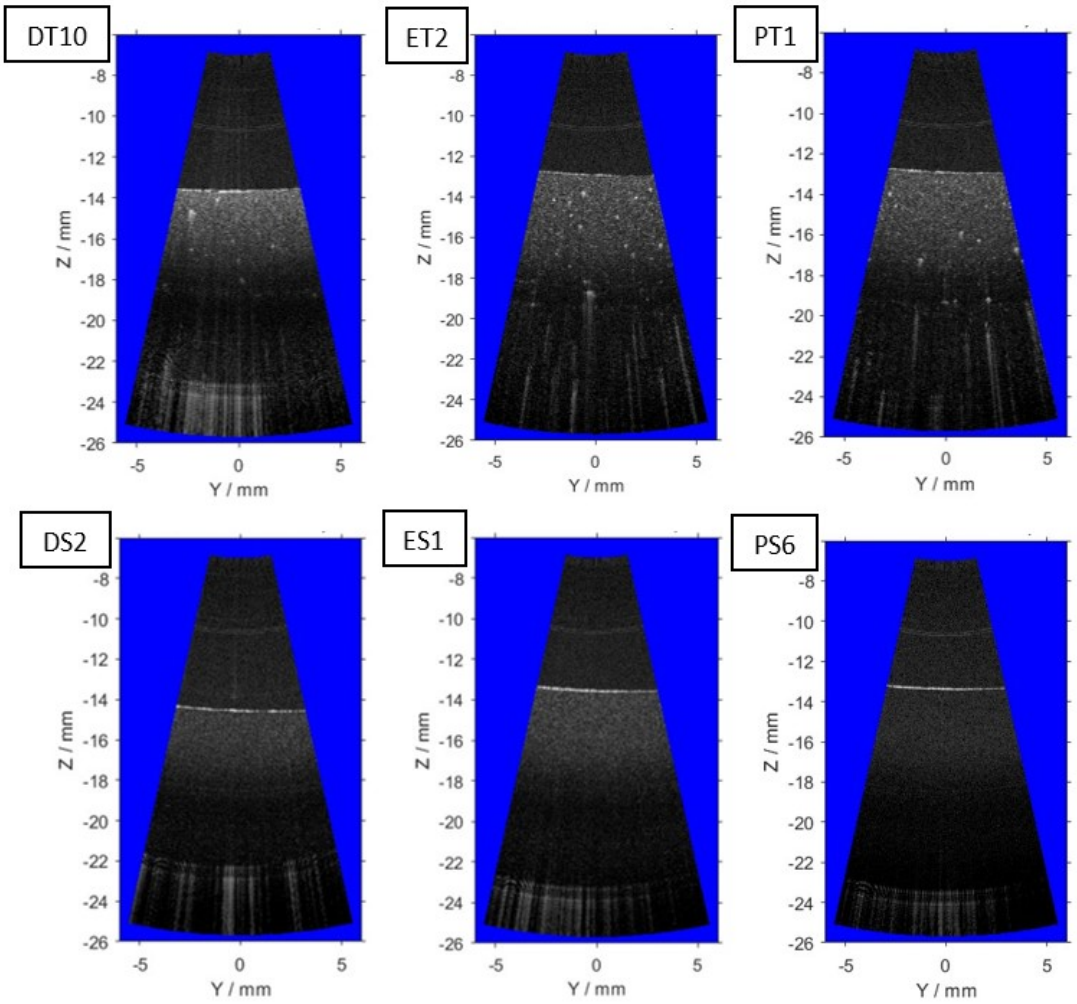

Figure (12) *For every condition of the test pieces the selected OCT scan is shown. The labels correspond with the names of the test pieces addressed in table 3. The bright (white) line around -13 mm in Z-direction represents the top surface of the test piece. Everything under this line represents the cross-section of the test piece. For every test piece the three-layered structure is not visible.*

6.1.2. Ultrasound

The representative ultrasound images of the six conditions addressed in section 6.1.1 are depicted in figure 13. These ultrasound scans have been used for the evaluation of the distinguishability between the layers. The scale of the ultrasound images is shown on the right side of the images. The total scale bar is 3 cm and the distance between the dots is 2 mm. The clear (bright) white line around 6 to 8 mm in depth represents the bottom surface of the test piece. The part of the ultrasound scan above this line is the image of the cross-section of the test piece. Regions with a higher scattering coefficient are depicted by regions with higher intensities in the ultrasound image. The ultrasound scans of all the test pieces show a clear three-layered structure, except for test piece PT1. The lines that represent the transition between the different layers of PT1 are visible but not clear.

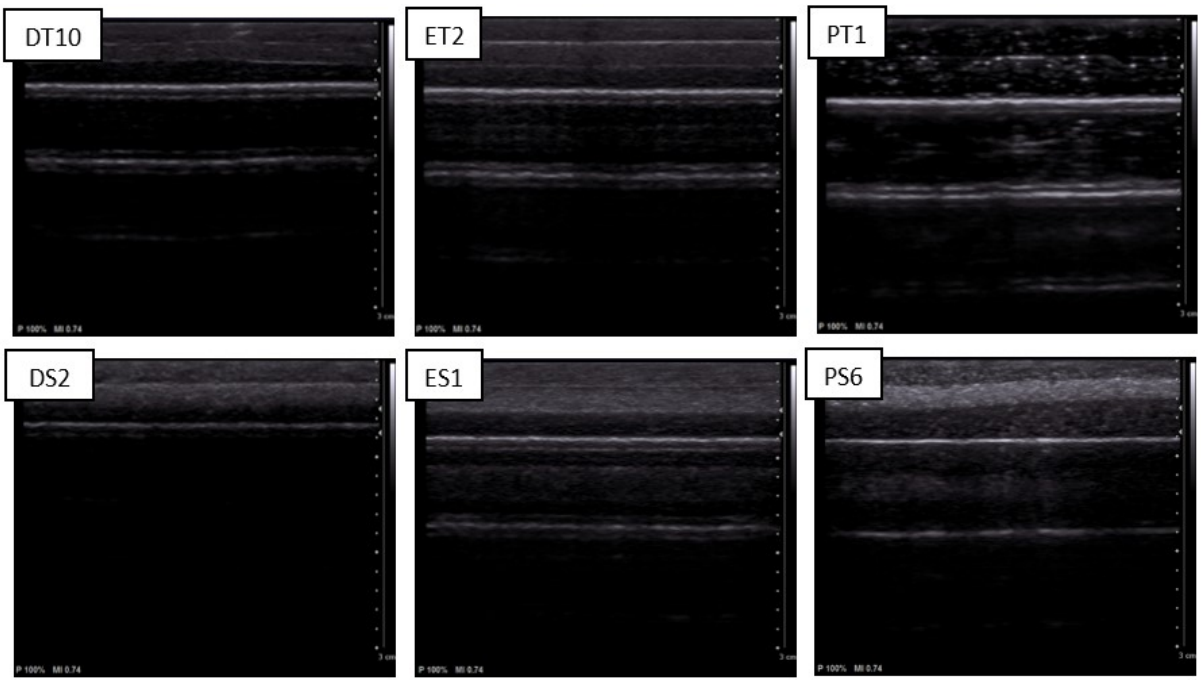

Figure (13) *For every condition of the test pieces the selected ultrasound scan is shown. The labels correspond with the names of the test pieces addressed in table 3. The bright (white) line around 6 to 8 mm in depth represents the bottom surface of the test piece. Everything above this line represents the cross-section of the test piece. The samples were scanned with the muscularis propria layer on top. Therefore, the order in which the layers are represented in the ultrasound scans from top to bottom are: muscularis propria, lamina propria and urothelium. The three-layered structure is clearly visible for every test piece, except for test piece PT1.*

The distinguishability of the layers is determined per condition by measuring the average intensity in grayscale per layer in ImageJ and comparing these intensities. ImageJ is an image processing software program based on Java. In grayscale an intensity of 0 represents the colour black and an intensity of 255 represents the colour white. The average intensities for the urothelium, lamina propria and muscularis propria and the ratio between these layers are given per condition in table 7. For every test piece the urothelium has the lowest intensity, lamina propria the highest and muscularis propria an intensity in between, except for DT10. The muscularis propria has a higher intensity than the lamina propria of DT10 and this is not desired. DS2 is the test piece with the biggest percentual difference in intensity between the urothelium and the lamina propria and ET2 with the smallest. The percentual difference in intensities between the muscularis propria and the lamina propria is the biggest for PS6 and relative small for DS2, ET2 and ES1, excluding PT1 and DT10 since these test

pieces did not result in the desired three-layered structure or intensity order. Therefore, in general PS6 has the best distinguishable three-layered structure evaluated by ultrasound.

Table (7) *For every condition of the test pieces the average intensity in grayscale per layer has been measured by ImageJ. The results, including the ratio between the average intensities, are shown in this table. U: urothelium. LP: lamina propria. MP: muscularis propria.*

	Average intensity U	Average intensity LP	Average intensity MP	Ratio average intensities U:LP:MP
DT10	6.2	33.6	38.8	1 : 5.4 : 6.3
ET2	21.9	46.4	40.1	1 : 2.1 : 1.8
PT1	8.2	28.4	16.3	1 : 3.5 : 2.0
DS2	9.8	56.4	48.7	1 : 5.8 : 5.0
ES1	20.9	61.8	51.6	1 : 3.0 : 2.5
PS6	29.4	96.4	62.3	1 : 3.3 : 2.1

6.2. Phantoms

Figure 14 contains pictures of the 5 phantoms that were created. For the evaluation of these phantoms multiple imaging techniques have been used, namely OCT, ultrasound and the miniature camera. The OCT and ultrasound scans should be analysed to determine whether or not the different layers in the phantoms can be distinguished and to determine the thickness of each layer. Furthermore, recordings made by the miniature camera are used to evaluate the texture of the inner surface of the phantoms.

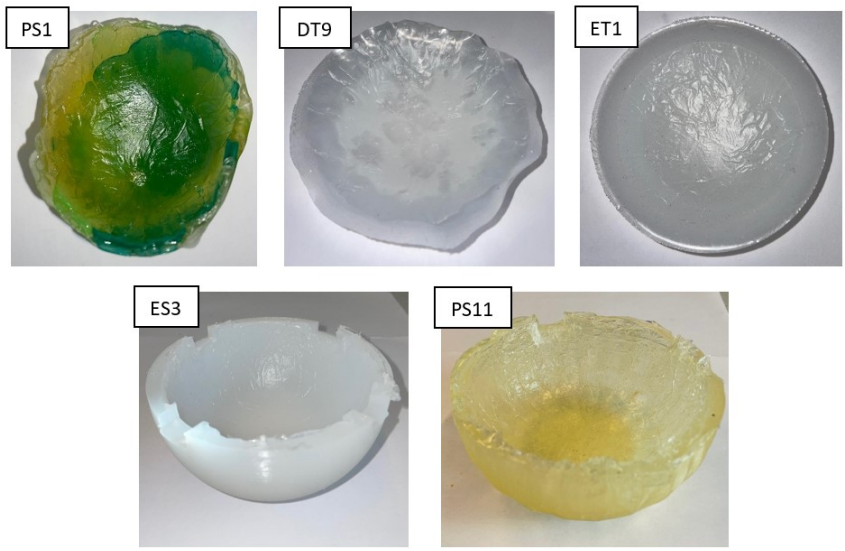

Figure (14) *Pictures of the 5 phantoms. The labels correspond with the names of the phantoms addressed in table 3. For the creation of phantoms PS1, DT9 and ET1 the mould was not completely filled with material. In contrast, phantoms ES3 and PS11 were made by filling the whole gap between the inner and outer part of the mould with material. Plastisol and silica are used to fabricate this three-layered phantom named PS1. Dragon Skin and titanium dioxide is used to fabricate this singular layered phantom named DT9. Ecoflex and titanium dioxide is used to fabricate this three-layered phantom named ET1. Ecoflex and silica is used to fabricate this three-layered phantom named ES3. Plastisol and silica is used to fabricate this three-layered phantom named PS11.*

6.2.1. OCT

Similar to the test pieces, a representative selection of phantoms was scanned by OCT. The OCT scans of these phantoms do not show the three-layered structure. This can be seen in figure 15. The bright (white) line that represents the inner surface of the phantoms can be seen in the OCT image at around -14 mm in Z-direction. The phantoms have a semi-spherical shape so when the phantoms are imaged from above the inner surface is scanned at an angle so the bright (white) line appears at an angle too. Just as with the test pieces, the OCT image of the phantom with titanium dioxide as scattering agent contains multiple high intensity spots and the OCT image of the phantom with silica as scattering agent does not.

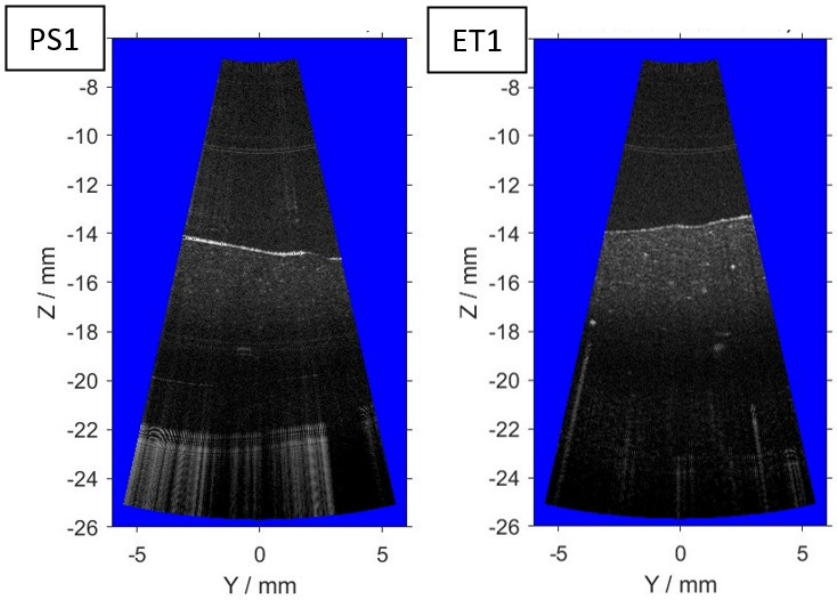

Figure (15) *For some phantoms the OCT scan is shown. The labels correspond with the names of the phantoms addressed in table 3. The bright (white) line around -14 mm in Z-direction represents the inner surface of the phantom. Everything under this line represents the cross-section of the phantom. For every phantom the three-layered structure is not visible.*

6.2.2. Ultrasound

For each phantom an ultrasound scan has been selected that represents the whole phantom. These ultrasound images are shown in figure 16. The ultrasound scans can be interpret similarly to that of the test pieces where the outer surface of the phantoms is represented by the bright (white) line around 8 to 12 mm in depth. The scale bar, on the right side of the ultrasound images, is in total 4 cm for the ultrasound images of phantoms PS1 and DT9 with a distance of 5 mm between the dots. The ultrasound images of phantoms ET1, ES3 and PS11 contain a 3 cm long scale bar where the distance between the dots is 2 mm. The three-layered structure was not visible in the ultrasound images of phantom ET1 and phantom DT9 has only one layer. Therefore the distinguishability and thicknesses cannot be determined for these phantoms.

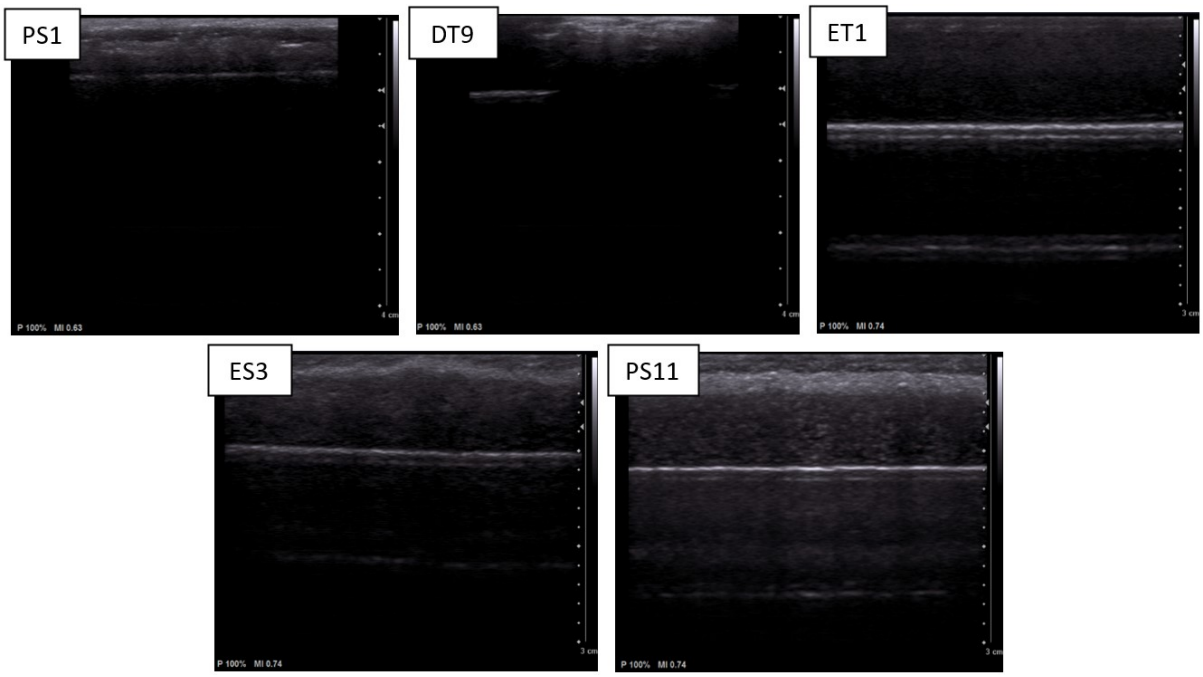

Figure (16) *For every phantom the selected ultrasound scan is shown. The labels correspond with the names of the test pieces addressed in table 3. The bright (white) line around 8 to 12 mm in depth represents the outer surface of the phantom. Everything above this line represents the cross-section of the phantom. The three-layered structure is clearly visible for three phantoms, but not for DT9 and ET1.*

Just as for the evaluation of the test pieces ImageJ has been used to evaluate the distinguishability between the layers in the phantom. The results of the intensity measurements are shown in table 8. It is important to note that the division of the intensities between the layers of phantom PS1 is not in accordance to that of a human bladder wall. Moreover, the specific concentrations of the scattering agents in the layers of phantom PS1 are unknown, since this is a first test phantom created solely to see if following the new production process results in a desired phantom. The ultrasound results of phantom PS1 are still relevant to show that the intensity can be adapted per layer, but this phantom cannot be used to draw specific conclusions from. In contrast to the other two phantoms for which the three-layered structure was visible, namely ES3 and PS11. For these phantoms the lamina propria contains the most scattering agent (3% w/w), followed by the muscularis propria (0.4% w/w) and the urothelium contains the least scattering agent (0.2% w/w). The ratio of the average intensities per layer are quite similar for phantoms ES3 and PS11. The percentual difference in intensities between the urothelium and the lamina propria is a bit bigger for ES3. However, the percentual difference in intensities between the lamina propria the muscularis propria is bigger for PS11 compared to ES3. Overall, the intensities are higher for the layers of PS11.

Moreover, the ultrasound scans have been used to evaluate the thicknesses of the different layers. This is done by measuring the thickness five times for each layer in ImageJ using the scale on the ultrasound images. An important remark is that the difference in velocities of sound in the different materials and human tissue has not been included in the thickness measurements. For a proper evaluation a correction needs to be implemented based on the relative speed of sound or calibration tests. The thickness measurements are used to calculate the average thickness and the standard deviation for all the phantom layers. These results including the ratio between the average thicknesses are shown in table 9. For every phantom, except for ES3, the order of least thick to

Table (8) *For every phantom the average intensity in grayscale per layer has been measured by ImageJ. The results, including the ratio between the average intensities, are shown in this table. The intensities could not be measured for phantoms DT9 and ET1, since these ultrasound images did not show the three-layered structure. U: urothelium. LP: lamina propria. MP: muscularis propria. n.a.: not applicable.*

	Average intensity U	Average intensity LP	Average intensity MP	Ratio average intensities U:LP:MP
PS1	104.7	46.4	48.2	1 : 0.4 : 0.5
DT9	n.a.	n.a.	n.a.	n.a.
ET1	n.a.	n.a.	n.a.	n.a.
ES3	54.0	92.7	30.3	1 : 1.7 : 0.6
PS11	65.8	102.2	33.4	1 : 1.6 : 0.5

thickest layer is urothelium, lamina propria and muscularis propria. For ES3 the urothelium is slightly thicker than the lamina propria. For PS1 the lamina propria is slightly larger than for PS11, both relative to the urothelium. PS1 contains the least thick muscularis propria and ES3 the thickest muscularis propria relatively to the urothelium and lamina propria. When the mean thicknesses of the layers are added the total thickness of the phantoms are 7.6, 9.7 and 11.7 mm for PS1, ES3 and PS11 respectively. The total thickness of PS1 complies the best with the 8 mm gap between the inner and outer part of the phantom mould. The layers of PS1 are of the most uniform thickness, since the standard deviations of the layers are the smallest for this phantom. The layers of ES3 differ the most in thickness when the standard deviations of the layers of this phantom are evaluated.

Table (9) *For every phantom five thickness measurements have been done in ImageJ per layer. The mean thickness, standard deviation and ratio between the average thicknesses are shown in this table. The thicknesses could not be measured for phantoms DT9 and ET1, since these ultrasound images did not show the three-layered structure. SD: standard deviation. U: urothelium. LP: lamina propria. MP: muscularis propria. n.a.: not applicable.*

	Mean thickness U ± SD (mm)	Mean thickness LP ± SD (mm)	Mean thickness MP ± SD (mm)	Ratio average thicknesses U:LP:MP
PS1	1.30 ± 0.21	1.55 ± 0.12	4.77 ± 0.08	1 : 1.2 : 3.7
DT9	n.a.	n.a.	n.a.	n.a.
ET1	n.a.	n.a.	n.a.	n.a.
ES3	1.05 ± 0.58	0.95 ± 0.05	7.70 ± 0.70	1 : 0.9 : 7.3
PS11	1.89 ± 0.14	2.13 ± 0.18	7.65 ± 0.26	1 : 1.1 : 4.0

6.2.3. Miniature camera

Pictures and videos were made of the inner surfaces of the phantoms by a miniature camera. A picture is shown in figure 17 for each phantom. These pictures are used to evaluate the texture of the phantoms seen by the miniature camera. The texture should represent the rugae of the bladder lining. In figure 17A a WLC image in grayscale is shown of an ex vivo pig bladder. This image can be used to compare the texture of the phantoms with. Phantoms PS1, ET1, ES3 and PS11 show a texture that is similar to that of the pig bladder. Randomly winding lines are seen on the inner surfaces of the phantoms, but these lines are grooves while the bladder lining consists of folds. However, because the miniature camera creates 2D images the difference between grooves and folds is hard to see, so the texture still looks similar. Phantom DT9 does not show any lines as can be seen in figure 17, since pockets of air entrapped in the phantom layer dominate the look of the inner surface of this phantom. The bladder lining does not show any pockets or holes, therefore the

texture of phantom DT9 does not comply with that of a bladder. Moreover, the grooves of the other phantoms are relatively deep and thick compared to the more subtle folds of the bladder lining.

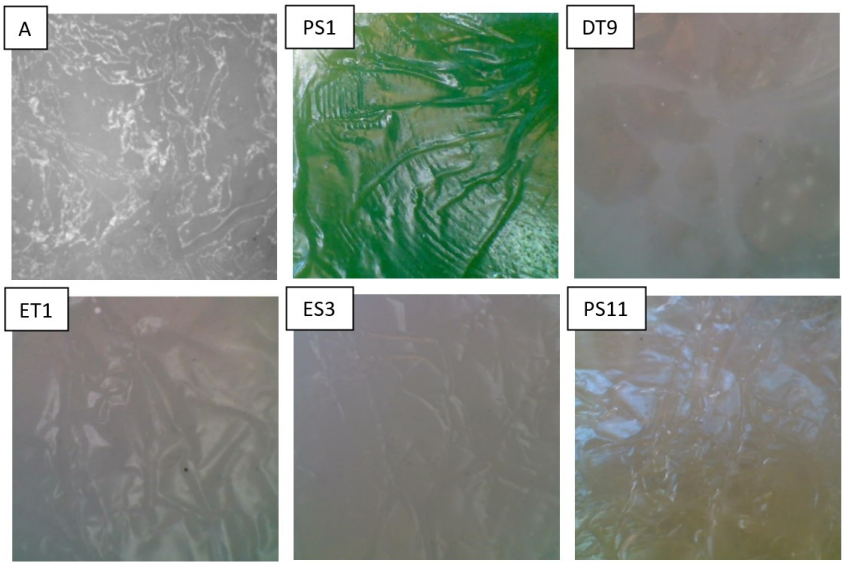

Figure (17) *Figure A shows an example of the lining of a bladder. It is a WLC image in grayscale of an ex vivo pig bladder. The folds that represent the rugae are visible. The other figures are pictures of the inner surface of the phantoms made by the miniature camera. The labels correspond with the names of the phantoms addressed in table 3. The texture is well visible for all the phantoms except for phantom DT9, since this phantom contains many air pockets in the phantom layer so the grooves are not visible.*

6.3. Tumour test pieces

See figure 18 for pictures of the 6 tumour test pieces. The tumour test pieces were scanned by OCT and ultrasound so the different tumour types that were created can be evaluated. The scans are used to compare the characteristics of bladder tumours to that of the tumour sites and to qualitatively evaluate if the tumours can be distinguished from healthy tissue in the tumour test pieces.

6.3.1. OCT

OCT scans were made of some tumour sites. These OCT images are shown in figure 19. Only two tumour test pieces were scanned, since two tumour test pieces were not fabricated yet when the OCT scans were made and the other two tumour test pieces did not contain any tumour sites. At around -13 mm in Z-direction the bright (white) line that represents the top surface of the tumour test piece can be seen in the OCT images of tumour test pieces PS7-dys and PS7-CIS in figure 19. In the OCT image of tumour test piece DT7-dys in figure 19 the clear transition between a region of low and high intensity represents the top surface of the tumour test piece. The absence of the three-layered structure in the OCT images is also applicable for the tumour test pieces. However, in figure 19 in the OCT image of tumour test piece DT7-dys the beginning of the thickening of the urothelium is indeed visible at the dysplasia tumour site. Similarly to the test pieces and phantoms, the OCT image of the tumour test piece that has titanium dioxide as scattering agent contains multiple high intensity spots while these spots are not visible on the OCT images of the tumour test piece with silica as scattering agent. Moreover, the intensity of the OCT images of the tumour test piece with silica as scattering agent is relatively low.

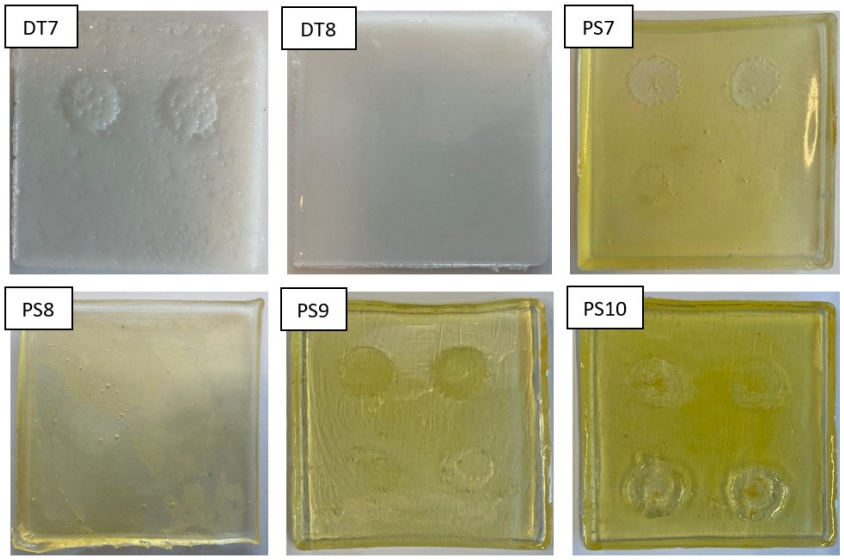

Figure (18) *Pictures of the 6 tumour test pieces. The labels correspond with the names of the tumour test pieces addressed in table 3. Dragon Skin and titanium dioxide are used to fabricate the two-layered tumour test piece named DT7, including tumour type dysplasia (top). Dragon Skin and titanium dioxide are used to fabricate the two-layered tumour test piece named DT8. Plastisol and silica are used to fabricate the three-layered tumour test piece named PS7, including tumour types dysplasia (top) and CIS (bottom). Plastisol and silica are used to fabricate the two-layered tumour test piece named PS8. Plastisol and silica are used to fabricate the three-layered tumour test piece named PS9, including tumour types dysplasia (top) and CIS (bottom). Plastisol and silica are used to fabricate the three-layered tumour test piece named PS10, including tumour types T1 (top) and T2 (bottom).*

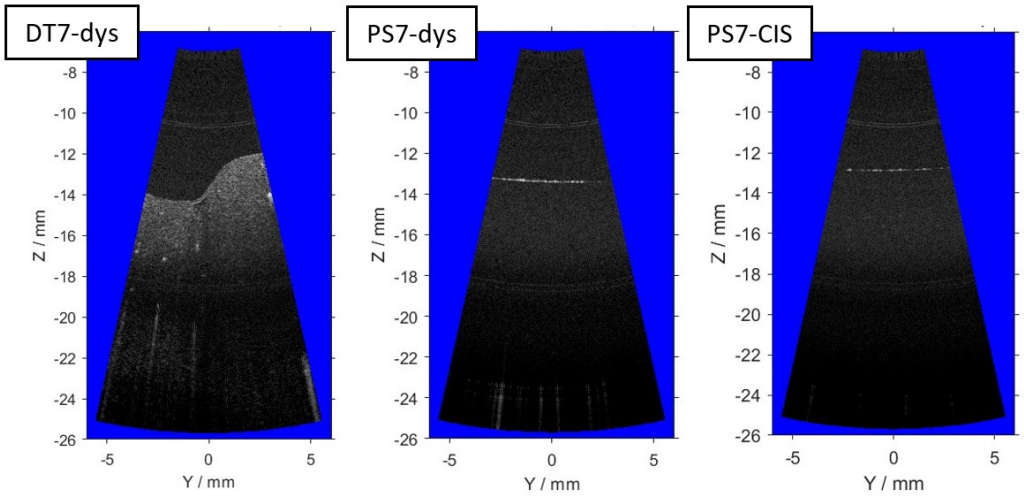

Figure (19) *For some tumour test pieces the OCT scan is shown. The labels correspond with the names of the tumour test pieces addressed in table 3 and the tumour type that is scanned in this tumour test piece, where dys is an abbreviation for dysplasia. Tumour test piece DT7 is two-layered and contains the dysplasia tumour type. Tumour test piece PS7 is three-layered and contains the dysplasia and CIS tumour type. In the OCT scans of tumour test pieces PS7-dys and PS7-CIS the bright (white) line around -13 mm in Z-direction represents the top surface of the tumour test piece. In the OCT scan of tumour test piece DT7-dys this is represented by the clear transition between a region of low and high intensity. Everything under the line or clear transition represents the cross-section of the tumour test piece. For every tumour test piece the three-layered structure is not visible, but the thickening of the urothelium for the dysplasia tumour site is shown in the OCT scan of tumour test piece DT7-dys.*

6.3.2. Ultrasound

For every tumour type present in the tumour test pieces an ultrasound scan has been selected. These ultrasound images are shown in figure 20. Tumour test pieces DT7-dys and DT8 are represented by ultrasound images with a scale bar of 4 cm and a distance between the dots of 5 mm. The scale bar for the other ultrasound images is 3 cm long and contains dots with a distance of 2 mm between them. The bright (white) line that represents the bottom surface of the test pieces are visible at around 4 mm for tumour test pieces DT7-dys, DT8 and PS8 in figure 20 and at around 8 mm for the other tumour test pieces in figure 20. This is because tumour test pieces DT7-dys, DT8 and PS8 contain only two layers and the others three layers, as is already discussed in section 5.6. Moreover, tumour test pieces DT8 and PS8 do not contain any tumour types since these tumour test pieces were made solely to see if the layers were visible. As can be seen in the figure 20 the two layers are better distinguishable for tumour test type PS8 than for DT8.

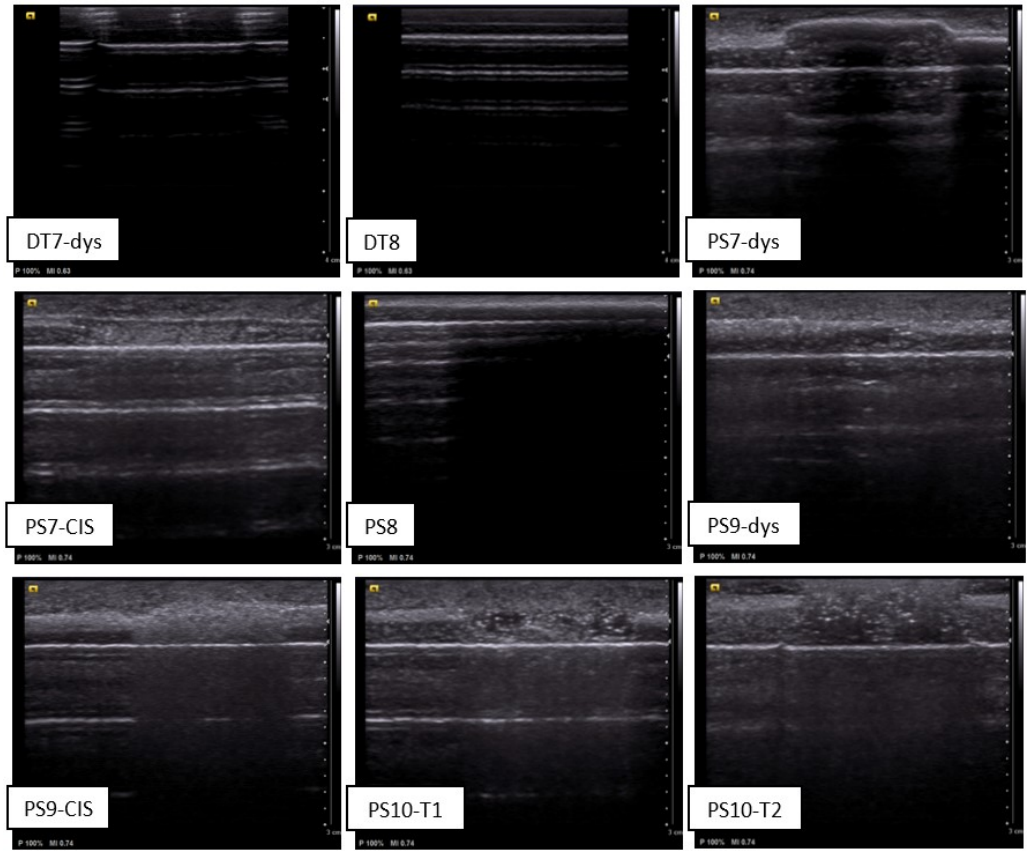

Figure (20) *For every tumour type in the tumour test pieces an ultrasound scan has been selected. The labels correspond with the names of the tumour test pieces addressed in table 3 and the tumour type that is scanned in this tumour test piece, where dys is an abbreviation for dysplasia. The bright (white) line around 4 or 8 mm in depth represents the bottom surface of the tumour test piece. Everything above this line represents the cross-section of the tumour test piece. Tumour test piece DT7 is two-layered and contains the dysplasia tumour type. Tumour test piece DT8 is two-layered and does not contain a tumour type. Tumour test piece PS7 is three-layered and contains the dysplasia and CIS tumour type. Tumour test piece PS8 is two-layered and does not contain a tumour type. Tumour test piece PS9 is three-layered and contains the dysplasia and CIS tumour type. Tumour test piece PS10 is three-layered and contains the T1 and T2 tumour type.*

6.3.2.1. Urothelial dysplasia

The tumour type urothelial dysplasia is showed in the ultrasound images of DT7-dys, PS7-dys and PS9-dys shown in figure 20. The thickening of the urothelium is best visible for PS7-dys. For DT7-dys the layers itself are not clearly visible and for PS9-dys only a very small thickened part of the bottom, darkest layer is depicted in the middle of the cross-section of the tumour test piece depicted in figure 20. The three-layered structure of the normal layers are clearly visible at the sides of the ultrasound scans of PS7-dys and PS9-dys as can be seen in figure 20, so the dysplasia can be well distinguished from the parts of the tumour test piece that represent the healthy tissue.

6.3.2.2. CIS

In figure 20 tumour type CIS is represented by PS7-CIS and PS9-CIS. In both figures a part of the urothelium has a lower intensity comparable to that of the lamina propria. However, this is visible more clearly for PS9-CIS. Since at the sides of the ultrasound images the urothelium has a much lower intensity the CIS tumour can be easily distinguished from the healthy three-layered structure.

6.3.2.3. T1

Tumour type T1 is represented by PS10-T1 in figure 20. The urothelium and lamina propria layers should transition from a high to a low intensity while the demarcation with the muscularis propria should remain clear to represent a T1 tumour. These characteristics can be seen in figure 20 for tumour test piece PS10-T1. However, the transition is not very smooth, the intensities are not uniformly shown but contain bright and dark spots and the demarcation with the muscularis propria is not very clear in the middle of the CIS tumour. Still, the tumour site can be well distinguished from the normal three-layered structure at the sides of the ultrasound images.

6.3.2.4. T2

Figure 20 contains the representation of the T2 tumour type by PS10-T2. For this tumour type the vertical structure should not be visible so there should be no clear demarcations between the layers while the intensity transitions from high at the urothelium to low at the muscularis propria. As can be seen in figure 20 at PS10-T2 the three-layered structure is not visible anymore at the tumour site, but it is visible at the sides of the ultrasound image. Therefore, the tumour can be clearly distinguished from the healthy tissue. However, similar to the T1 tumour type the transition form high to low intensity is not completely smooth and the intensities are not horizontally evenly distributed but contain spots at the lower intensities.

7. Discussion

The results are discussed and compared to what can be found in literature. Thereby explanations for unexpected findings, limitations and recommendations are given. Lastly, improvements for the phantom as well as further research are addressed. For clarity, the discussion is divided into several sections.

7.1. OCT

OCT is one of the two imaging techniques used by the robot-controlled catheter developed for the Next-Gen In-Vivo project. Unfortunately, the phantoms that are described in this report did not show a representation of the characteristics of a human bladder by OCT imaging. Namely, no layers of different intensities were visible when the phantoms, or (tumour) test pieces, were scanned by OCT as can be seen in figures 12, 15 and 19. A plausible explanation for this can be that the samples were too thick. For the test pieces and tumour test pieces a method was chosen to create layers of 2, 2 and 4 mm for the urothelium, lamina propria and muscularis propria respectively. However, the penetration depth of OCT is limited to 2 to 3 mm [11, 12]. Therefore, when the (tumour) test pieces were imaged by OCT it is possible that the transition from the urothelium to the lamina propria was not visible, since this transition takes place around 2 mm in depth which is around the penetration depth of OCT. If this is the case it is logical why only a single intensity region is shown on the OCT scans of the (tumour) test pieces, namely then only the urothelium layer is visible. This complies with the intensity shown in the OCT scans in figures 12 and 19, since the urothelium should create a region with a low intensity and the OCT images depict a cross-section that is quite dark coloured.

Moreover, the scans of the two phantoms also did not contain any layered structure. For phantom ET1 this can be expected considering that the ultrasound scan in figure 16 also did not show any layers and the technique of OCT and ultrasound are comparable [11]. The urothelium layer of phantom PS1 is around 1.3 mm thick, less than the penetration depth of OCT [11, 12]. However, the transition to the lamina propria layer is not visible in the OCT image of phantom PS1 in figure 15. This can be explained by knowing that the concentration of the scattering agent in the urothelium of phantom PS1 is not precisely known, but it is known that during the creation a relatively high concentration of scattering agent was added to this phantom compared to other samples. Besides, as can be seen in the ultrasound image of phantom PS1 in figure 16 and in table 8 the alternation of intensities is switched for the layers, so the urothelium has the highest scattering coefficient. This means that the upper layer of the imaged phantom PS1 contains a lot of reflective parts which results in the reflection of a great proportion of the light send by the OCT probe. Only a small amount of the light will reach deeper than the urothelium layer, so the layers underneath cannot be visualised well [11, 12]. This gradual reduction of reachability of light in depth must be considered when a sample is created that will be scanned by OCT, so this does not affect the desired absolute intensities of the more deeper layers on OCT images.

It is necessary to scan more different phantoms by OCT to investigate the way the varying properties of these phantoms and its layers are represented on OCT images. For this further research it is recommended to adapt the fabrication process to achieve less thick layers and thereby reducing the total thickness of the newly created phantoms to less than the penetration depth of OCT. This is necessary, because based on the thicknesses of the urothelium layers of the phantoms written in table 9 it is questionable if the transition between the urothelium and the lamina propria would be visible even if all the other factors, for example scattering agent concentrations, are ideal. This applies to all the phantoms that were created during this assignment. Therefore, a new fabrication

method should be used or the number of layers of aluminium foil wrapped around the inner part of the mould should be reduced to create thinner layers. Next to that the gap between the inner and outer part of the mould should be reduced to around 2 mm to achieve a total thickness of the phantom wall that is similar to the penetration depth of OCT.

Another problem that occurred during the OCT imaging is that the surface of the samples were relatively reflective. The this can be seen in figures 11, 14 and 18 where the reflection of the flash used to take the pictures is clearly visible for some of the samples. This reflective behaviour is represented in the OCT scans by the very bright white line. The white line represents the surface of the samples and the brightness indicates that a lot of light is reflected on this surface [11, 12]. If a great proportion of the light is reflected directly on the surface this light is lost and cannot reach into the sample what causes problems with the intensities and therefore visibility of the samples structure in depth. This phenomenon is similar to what has already been discussed about the possible problem with imaging phantom PS1. To reduce the reflective behaviour of the samples and therefore improve the OCT imaging results the surface of the samples should be more bent and not flat, a less reflective material should be used or surface treatment should be applied to rougher the surface.

When the OCT scans were made it was noted that some of the scans were blurry. By inspecting the scanning process it has been found out that the 0.1 mm movement of the scanning table to position the sample for the next cross-sectional scan will induce a movement of the sample too. Sometimes the sample still shook while the next scan is already being made what resulted in a blurry scan. To prevent this a stiffer material should be used for the samples or the time span between moving the scanning table and starting the next scan should be increased.

7.2. Dragon Skin

As became clear from the literature study, previous research has been done about creating a bladder phantom with Dragon Skin as the base material [8]. In the article the researchers state that the fastest curing Dragon Skin was used, which has a pot life of 4 minutes and a curing time of 30 minutes. For the creation of the samples described in this report Dragon Skin with a pot life of 8 minutes and a curing time of 75 minutes has been used. Although this is longer than used for the research of G.T. Smith et al. the curing time appeared too short when the samples were fabricated. Air bubbles inside the mixture of base material and scattering agent could not be removed properly before the mixture started to cure. During this assignment factors other than the short curing time that could have influenced the results of the Dragon Skin phantoms were investigated. An increase in concentrations of the scattering agents, an increase in the difference of scattering agent concentrations between layers or the use of silica instead of titanium dioxide did not lead to the desirable results of a clear three-layered phantom made of Dragon Skin. Sometimes the three layers or only the transition between the three layers are visible on the ultrasound images of Dragon Skin samples, but the desirable intensity ratio between layers was never achieved as can be concluded from the results in table 7.

Moreover, the viscosity increased rapidly after mixing part A and B of the Dragon Skin what resulted in a substance that could not be poured in a mould but had to be scraped out of the mixing beaker into the mould. For the creation of the (tumour) test pieces the substance had to be flattened over the whole surface of the container, since the mixture did not flow and thereby did not evenly cover the surface by itself. This complication and that of the short curing time could explain why the samples made of Dragon Skin did not show the best layered structure in the ultrasound images in figures 13, 16 and 20. It is possible that the phantom made by G.T. Smith et al. showed a better representation of the layers of a human bladder, because a better and faster vacuum machine was

being used or a shorter mixing time was implemented so more time would be left to remove the air bubbles and to use the material for the creation of the phantom before it cured [8].

7.3. EcoFlex

In contrast to using Dragon Skin, it is possible to remove the air bubbles in the vacuum machine after mixing the scattering agent into Ecoflex and before pouring the mixture in the mould. This is because the EcoFlex that has been used has a long enough curing time. However, a disadvantage of the long curing time might be that the scattering agent will settle at the bottom of the mixture and therefore is not evenly distributed in the mixture anymore. Although this is not visible in the ultrasound images in figure 13, since every layer appears with a uniform intensity. More research is needed to determine the ideal curing time. Preferably the curing time should be as short as possible to reduce the fabrication process time, but a balance has to be found so the curing time is long enough for the mixture to remain pourable and it is still possible to properly remove the air in the mixture.

EcoFlex differs from the other base materials in more aspects than the curing time. For example, EcoFlex is less elastic and less strong than Dragon Skin [27]. The values of these properties comply more with the characteristics of a human bladder for Dragon Skin than for EcoFlex [33]. This means that it is relevant to investigate the possibilities with a longer curing time Dragon Skin than used for this research. Thereby, the properties that lead to a more desirable result according to this report like the longer curing time of EcoFlex and the elasticity and strength of Dragon Skin are combined.

7.4. Plastisol

The curing time of plastisol is even shorter than that of Dragon Skin. This results in phantoms where the bottom part is significantly thicker than the upper parts, since the plastisol cures almost instantly after it has been poured into the bottom of the outer part of the mould so there is not enough time for the mixture to be pushed up in the gap between the inner and outer part of the mould. However, the problems regarding removing the air inside the mixture are less prominent for the fabrication of the (tumour) test pieces as can be concluded from the absence of visible air pockets in the pictures in figures 11 and 18 and in the ultrasound images in figures 13 and 20. The air that is entrapped in the plastisol before it has been heated and mixed with a scattering agent can be well removed in a vacuum machine. Only the air that is entrapped because of mixing the scattering agent into the plastisol cannot be removed properly, but this air is mostly pushed out of the mixture while heating the plastisol because of the high temperature. Therefore, for the creation of the (tumour) test pieces the appearance of air bubbles is not a big problem when the mixture is carefully poured in the container.

On the contrary, for the creation of phantoms entrapment of air is a problem. Air pockets can be seen in the pictures of plastisol phantoms in figure 14. The force of pushing the inner part of the mould into the outer part of the mould results in pushing the mixture up in the gap whereby air gets entrapped in the mixture. Normally with other base materials these air pockets also get pushed out, but the air does not have time to escape before the plastisol cures. This problem can be solved by heating up the vacuum machine oven. After the plastisol has been heated outside the vacuum machine oven and the scattering agent has been mixed into the plastisol, the mixture can be put in the heated vacuum machine oven so the air resulting from mixing can be removed without cooling the plastisol down and thereby preventing the plastisol form curing yet. Also, it can be investigated if it is possible to mix the scattering agent in the plastisol before the plastisol is heated up. Then

the air in the scattering agent plastisol mixture can be removed in a vacuum machine before the mixture is heated so the air that is entrapped in the mixture because of mixing is gone. However, for both solutions research is needed to investigate whether or not the scattering agent settles at the bottom of the mixture during the quite lengthy process from mixing the scattering agent into the plastisol and pouring it in the mould. If the scattering agent does settle the distribution within the mixture gets disrupted which negatively influences the appearance of the uniform intensities per layer.

A disadvantage of plastisol is the temperature of the mixture before it can be poured into the mould. The mixture is heated up to 240°C which causes the 3D printed mould to slightly melt and thereby deform. The material of the 3D printed mould cannot withstand the heat and since most of the mould is only filled for 10% the inner volume of the mould consists mostly of air which does not dissipate the heat well. When significant deformations occur the mould cannot be used since the inner and outer part of the mould will not fit into each other anymore. Therefore, developing a heat-resistant mould would be a necessity if plastisol is being used as the base material for a phantom. An advantage of plastisol is that a desired elasticity can be achieved, for example that of a human bladder wall, when the soft, medium and strong versions of plastisol are mixed in the right ratio.

7.5. Titanium dioxide

Titanium dioxide did not work very well as a scattering agent for the creation of the samples described in this report. The titanium dioxide particles did not dissolve in the base material, but stayed in clusters. This resulted in high intensity spots that appeared on the OCT and ultrasound images in figures 12, 13, 15 and 19. In previous research titanium dioxide has been used many times as a scattering agent [8, 9, 17, 29, 31, 32]. It has been mixed with different base materials including Dragon Skin and plastisol. Therefore, it is unexpected that the mixing of titanium dioxide did not turn out as desired during this assignment. It is possible that a titanium dioxide with a different crystal structure has been used than in literature. Moreover, extra steps could have been implemented like sonication to loosen the titanium dioxide particles. Or the mixing of the titanium dioxide took place at an adjusted temperature or pressure in previous research so the titanium dioxide particles dissolved better. It was remarkable that the titanium dioxide already clumped in its container so maybe it was not stored under the right conditions.

G.T. Smith et al. investigated the concentrations of titanium dioxide that needed to be added to Dragon Skin to create the exact scattering coefficients of the different bladder wall layers [8]. However, when these concentrations were applied the samples made of Dragon Skin did not show the desired three-layered structure. This could be because of the complications of Dragon Skin as already discussed or because ultrasound was used to image the samples instead of OCT. The different properties of OCT compared to ultrasound could have made it possible that the concentrations described in literature would lead to a desired result. Unfortunately, this could not be tested during this assignment, since scanning with OCT did not result in the expected images. Furthermore, the described concentrations are based on mixing titanium dioxide into Dragon Skin. When other base materials or scattering agents are used with other optical properties the described concentrations will not comply with the exact scattering coefficients of the different bladder wall layers. The different concentrations per layer have to be investigated per base material scattering agent combination to achieve the desired scattering coefficients.

7.6. Silica

When silica was used as a scattering agent no clumps were formed as with titanium dioxide. The intensities are more uniformly distributed as can be seen in the OCT and ultrasound images of samples made with silica in figures 12, 13, 15, 16, 19 and 20. One of the reasons that silica might dissolve well is that the silica particle size is 60 to 200 µm which is relatively small and the particles did not cluster in the storage jar. To achieve the desired three-layered structure higher weight by weight percentages were used than were described for titanium dioxide mixed into Dragon Skin in research done by G.T. Smith et al. [8]. However, this is expected since silica has a lower refractive index than titanium dioxide so a higher concentration of silica is needed to achieve the same scattering coefficient as with titanium dioxide [30, 31]. Also the difference in concentrations of silica between layers needed to be higher for a proper distinguishment.

7.7. Tumour sites

For the creation of the tumour sites methods described in literature were used [9]. The tumour test pieces that were created did show most of the tumour type characteristics, but the tumour sites could still be improved. As can be seen in figure 20 not all tumour types appeared clearly on the ultrasound images. To create a proper transition zone in tumour types T1 and T2 another base material than plastisol should be used since plastisol cured too fast before the layers could be properly stirred. The tumour test pieces made of Dragon Skin and titanium dioxide did not turn out as is desired, probably because of the complications that are already discussed. Moreover, the tumour test pieces that contained silica also appeared with bright spots on the ultrasound images in figure 20 comparable to samples made with titanium dioxide. It is possible that the silica did not distribute well, because only a small amount of mixture was prepared for filling up the tumour sites. This small amount only lead to a small layer in the container the mixture was heated and mixed in and therefore the silica could not get distributed evenly since there was no volume to flow through the whole mixture.

7.8. Phantom improvements

Improvements regarding imaging by OCT, the thickness of the layers and the optical characteristics of the tumour types are already discussed. However, more improvements could be made so the phantom would comply with all the requirements and wishes. For instance, the phantoms shape and size could be adjusted so it resembles the human bladder more and tubes that represent the urethra and ureters could be added for better anatomical resemblance. These improvements could also help with the betterment of the representation of the physiology of the human bladder. Especially if the phantom would be made of material that has the same elastic properties as a human bladder. To enhance the pathological representation the tumour types should be integrated within the phantom instead of in separate tumour test pieces. The visual characteristics of bladder tumours as well as the bladder wall in general should be added, such as redness and thickening of the tumour sites and blood vessels. In figure 17 the pictures of the inner surface of the phantoms are shown. The texture of the phantoms does resemble the texture of a human bladder, but the texture can be improved by making folds instead of grooves and by making the texture more subtle. Furthermore, the fabrication process must be adapted so no material can flow in between the aluminium foil layers and the inner part of the mould. Then, the thickness of the phantom wall will be more constant, since the extra space between the aluminium foil layers and the inner part of the mould decreases the thickness of the phantom wall at that spot. Moreover, the phantom got stuck in the mould

because the phantoms material directly flowed onto the inner part of the mould which caused it to stick to the mould. If this is prevented it would be a lot easier to remove the phantom from the mould. In addition, the exact scattering agent concentrations should be found per layer so the scattering coefficients of the phantoms layers are the same as that of human bladder wall layers. Thereby the evaluation of the three-layered structure should not be done by determining the ratio of the intensities between the layers, but by evaluating the absolute scattering coefficients of the layers. Lastly, the distinguishability of the layers should not be tested by ultrasound, but by OCT during the fabrication process.

7.9. Further research

Some recommendations for further research are already addressed, like developing another fabrication process, investigating the results of a phantom made out of Dragon Skin with a longer curing time, creating tumour types made of a different material than plastisol, finding the base material scattering agent combination that will result in a phantom with similar elasticity properties as a human bladder preferably by testing it by filling the phantom with liquid whereafter the phantom is emptied and determining the scattering agent concentrations for each base material scattering agent combination to achieve the exact same scattering coefficients as the bladder wall for each layer. However, even more further research can be thought of considering the results of this report. Most importantly, no specific base material scattering agent combination has been found that results in the desired phantom. Therefore, more different base materials and scattering agents should be researched to see if a new combination will improve the results. Finally, the shelf life of the phantoms should be further investigated.

8. Conclusion

Several phantoms were created that show the representation of the different layers of the human bladder wall on ultrasound scans. When the combinations of the different base materials (Dragon Skin, Ecoflex and plastisol) and scattering agents (titanium dioxide and silica) were compared the plastisol-silica combination showed the best distinguishable layers and the Ecoflex-silica phantom showed the most representative three-layered structure regarding thicknesses of the layers. Both samples contain layers with scattering agent concentrations of 0.2, 3 and 0.4 % w/w to represent the urothelium, lamina propria and muscularis propria layer respectively.

Besides the phantoms, test pieces that include different bladder tumour types were made. Several tumorous characteristics are visible when the tumour test pieces were scanned by ultrasound, but the tumours should be integrated in the phantom for optimal useability.

A new fabrication process has been tested and worked well to create layers in a relatively accessible and easy way. In contrast with existing methods for the creation of (bladder) phantoms which use advanced techniques or take a long time to execute. Also, the developed fabrication method includes adding texture to the phantom that represents the lining of a human bladder. This texture can be seen on images made by a miniature camera. However, the phantoms that are created by following the described fabrication process cannot be used for testing with OCT imaging yet. Therefore, further improvements have to be made. The most important improvements are adjusting the fabrication process so even thinner layers can be fabricated and creating a less reflective surface of the phantoms.

In general, prototypes have been developed of phantoms that would be suitable to do experiments with using the robot-controlled catheter of the Next-Gen In-Vivo project. Several improvements were made compared to the previous phantom regarding the addition of optical and visual characteristics of a human bladder. Finally, the results of this report can be used to optimize the phantom with the end goal to create a proper testing environment so diagnostic techniques can be enhanced and thereby the experience and results for patients with bladder cancer improved.

Acknowledgements

I would like to thank dr. F.J. Siepel, dr. V. Groenhuis and dr. M. Dantuma for taking place in my bachelor assignment committee and an extra thank you to my daily supervisor, dr. V. Groenhuis, who I had weekly meetings with, who I could ask my questions and provided feedback on my report. Moreover, the people of Scinvivo deserve my gratitude for providing, setting up and helping with the OCT scanning device. Also, my thanks to the students and supervisors of the RaM group who I had biweekly meetings with and talked to in the lab about our assignments. Furthermore, I would like to thank J.M. Boelema-Kaufmann for providing support as the RaM secretary. The RaM technicians deserve my appreciation too, for ordering my materials and for providing help in the lab where needed. I would like to mention dr. E.B. Cornel for his insights as a urologist. Lastly, my thanks to the University of Twente for the opportunity to fulfil my bachelor assignment at one of the research groups of the university.

References

[1] World Cancer Research Fund International. *Bladder cancer statistics*. URL: https://www.wcrf.org/cancer-trends/bladder-cancer-statistics/. (accessed: 28.06.2022).

[2] Cancer.Net Editorial Board. *Bladder Cancer: Statistics*. URL: https://www.cancer.net/cancer-types/bladder-cancer/statistics. (accessed: 28.06.2022).

[3] Robotics and Mechatronics. *NEXTGENINVIVO: Next Gen In-Vivo Cancer Diagnostics*. URL: https://www.ram.eemcs.utwente.nl/research/projects/nextgeninvivo. (accessed: 28.06.2022).

[4] Srinivasa Rao Bolla, Nkiruka Odeluga, and Raghu Jetti. "Histology, Bladder". In: *StatPearls [Internet]*. StatPearls Publishing, 2022.

[5] MD Matthew Hoffman. *Picture of the Bladder*. URL: https://www.webmd.com/urinary-incontinence-oab/picture-of-the-bladder. (accessed: 28.06.2022).

[6] Paul M. Heidger Ronald A. Bergman Adel K. Afifi. *Atlas of Microscopic Anatomy: Section 12 - Urinary System Plate 12.242 Urinary Bladder*. URL: https://www.anatomyatlases.org/MicroscopicAnatomy/Section12/Plate12242.shtml. (accessed: 28.06.2022).

[7] Cancer.Net Editorial Board. *Bladder Cancer: Stages and Grades*. URL: https://www.cancer.net/cancer-types/bladder-cancer/stages-and-grades. (accessed: 28.06.2022).

[8] Gennifer T Smith et al. "Multimodal 3D cancer-mimicking optical phantom". In: *Biomedical optics express* 7.2 (2016), pp. 648–662.

[9] Gennifer T Smith et al. "Multilayered disease-mimicking bladder phantom with realistic surface topology for optical coherence tomography". In: *Design and Performance Validation of Phantoms Used in Conjunction with Optical Measurement of Tissue VI*. Vol. 8945. SPIE. 2014, pp. 101–108.

[10] Antonio Lopez-Beltran et al. "Urothelial dysplasia of the bladder: diagnostic features and clinical significance." In: *Analytical and quantitative cytopathology and histopathology* 35.3 (2013), pp. 121–129.

[11] James G Fujimoto et al. "Optical coherence tomography: an emerging technology for biomedical imaging and optical biopsy". In: *Neoplasia* 2.1-2 (2000), pp. 9–25.

[12] Silke Aumann et al. "Optical coherence tomography (OCT): principle and technical realization". In: *High Resolution Imaging in Microscopy and Ophthalmology* (2019), pp. 59–85.

[13] Steven L Jacques. "Optical properties of biological tissues: a review". In: *Physics in Medicine & Biology* 58.11 (2013), R37.

[14] JE Freund et al. "Optical coherence tomography in urologic oncology: a comprehensive review". In: *SN Comprehensive Clinical Medicine* 1.2 (2019), pp. 67–84.

[15] O'tega Ejofodomi. "Measurement of optical scattering coefficient of the individual layers of the human urinary bladder using optical coherence tomography". In: *ISRN Biomedical Imaging* 2014 (2014).

[16] A Karl et al. "Optical coherence tomography for bladder cancer-ready as a surrogate for optical biopsy?-results of a prospective mono-centre study". In: *European journal of medical research* 15.3 (2010), pp. 131–134.

[17] Kristen L Lurie et al. "Three-dimensional, distendable bladder phantom for optical coherence tomography and white light cystoscopy". In: *Journal of biomedical optics* 19.3 (2014), p. 036009.

[18] Carmel M Moran and Adrian JW Thomson. "Preclinical ultrasound imaging—A review of techniques and imaging applications". In: *Frontiers in Physics* (2020), p. 124.

[19] Antonina I Volikova et al. "Structural, biomechanical and hemodynamic assessment of the bladder wall in healthy subjects". In: *Research and Reports in Urology* 11 (2019), p. 233.

[20] Vikram Chalana et al. "Automatic measurement of ultrasound-estimated bladder weight (UEBW) from three-dimensional ultrasound". In: *Reviews in Urology* 7.Suppl 6 (2005), S22.

[21] Alison H Blatt, Jehan Titus, and Lewis Chan. "Ultrasound measurement of bladder wall thickness in the assessment of voiding dysfunction". In: *The Journal of urology* 179.6 (2008), pp. 2275–2279.

[22] J.L. Richenberg. *Clinical Ultrasound*. 3rd ed. London UK: Churchill Livingstone, 2011.

[23] Roger Chou et al. "Comparative effectiveness of fluorescent versus white light cystoscopy for initial diagnosis or surveillance of bladder cancer on clinical outcomes: systematic review and meta-analysis". In: *The Journal of urology* 197.3 (2017), pp. 548–558.

[24] Yair Lotan et al. "Blue light flexible cystoscopy with hexaminolevulinate in non-muscle-invasive bladder cancer: review of the clinical evidence and consensus statement on optimal use in the USA—update 2018". In: *Nature Reviews Urology* 16.6 (2019), pp. 377–386.

[25] University of Michigan Health Rogel Cancer Center. *Blue Light Cystoscopy*. URL: `https://www.rogelcancercenter.org/bladder-cancer/diagnosis-and-treatment/blue-light-cystoscopy`. (accessed: 20.07.2022).

[26] Department of Urology University of Virginia School of Medicine. *Blue Light Fluorescent Cystoscopy*. URL: `https://med.virginia.edu/urology/for-patients-and-visitors/kidney-cancer/blue-light-fluorescent-cystoscopy/`. (accessed: 20.07.2022).

[27] Eunjin Choi et al. "Soft urinary bladder phantom for endoscopic training". In: *Annals of Biomedical Engineering* 49.9 (2021), pp. 2412–2420.

[28] A Ejofodomi O'tega, Vesna Zderic, and Jason M Zara. "Tissue-mimicking bladder wall phantoms for evaluating acoustic radiation force-optical coherence elastography systems". In: *Medical physics* 37.4 (2010), pp. 1440–1448.

[29] H Günhan Akarçay et al. "Determining the optical properties of a gelatin-TiO 2 phantom at 780 nm". In: *Biomedical optics express* 3.3 (2012), pp. 418–434.

[30] Jason R Cook, Richard R Bouchard, and Stanislav Y Emelianov. "Tissue-mimicking phantoms for photoacoustic and ultrasonic imaging". In: *Biomedical optics express* 2.11 (2011), pp. 3193–3206.

[31] Daniel Martijn M de Bruin et al. "Optical phantoms of varying geometry based on thin building blocks with controlled optical properties". In: *Journal of biomedical optics* 15.2 (2010), p. 025001.

[32] S Chatelin et al. "Polyvinyl chloride-plastisol: a soft tissue-mimicking phantom dedicated to multi-modality elastography". In: *SPIE Photonics West*. 2020.

[33] Niall F Davis et al. "Urinary bladder vs gastrointestinal tissue: a comparative study of their biomechanical properties for urinary tract reconstruction". In: *Urology* 113 (2018), pp. 235–240.